



저작자표시-비영리-변경금지 2.0 대한민국

이용자는 아래의 조건을 따르는 경우에 한하여 자유롭게

- 이 저작물을 복제, 배포, 전송, 전시, 공연 및 방송할 수 있습니다.

다음과 같은 조건을 따라야 합니다:



저작자표시. 귀하는 원저작자를 표시하여야 합니다.



비영리. 귀하는 이 저작물을 영리 목적으로 이용할 수 없습니다.



변경금지. 귀하는 이 저작물을 개작, 변형 또는 가공할 수 없습니다.

- 귀하는, 이 저작물의 재이용이나 배포의 경우, 이 저작물에 적용된 이용허락조건을 명확하게 나타내어야 합니다.
- 저작권자로부터 별도의 허가를 받으면 이러한 조건들은 적용되지 않습니다.

저작권법에 따른 이용자의 권리는 위의 내용에 의하여 영향을 받지 않습니다.

이것은 [이용허락규약\(Legal Code\)](#)을 이해하기 쉽게 요약한 것입니다.

[Disclaimer](#)

Master's Thesis

Loop Thermosyphon Performance and Flow Instability

Geunchan Lee

Department of Mechanical Engineering

Graduate School of UNIST

2019

Loop Thermosyphon Performance and Flow Instability

Geunchan Lee

Department of Mechanical Engineering

Graduate School of UNIST

Loop Thermosyphon Performance and Flow Instability

A thesis/dissertation
submitted to the Graduate School of UNIST
in partial fulfillment of the
requirements for the degree of
Master of Science

Geunchan Lee

07. 17. 2019 Month/Day/Year of submission

Approved by

A handwritten signature in black ink, appearing to read 'Jaeseon Lee', is written over a horizontal line.

Advisor

Jaeseon Lee


Loop Thermosyphon Performance and Flow Instability

Geunchan Lee

This certifies that the thesis/dissertation of Geunchan Lee is approved.

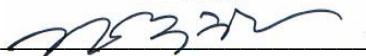
07. 17. 2019 Month/Day/Year of submission

signature



Advisor: Jaeseon Lee

signature



Jooha Kim: Thesis Committee Member #1

signature



Gunho Kim: Thesis Committee Member #2

signature

typed name: Thesis Committee Member #3

signature

typed name: Thesis Committee Member #4

three signatures total in case of masters

Abstract

The effects of the condenser type on the thermosyphon performance characteristics and the instability of the circulation flow were experimentally analyzed. Two types of condensers, shell-and-tube condenser and trapezoid reflux condenser were applied to the loop thermosyphon to compare its thermal performances and flow characteristics. The performance of loop thermosyphon was investigated according to working fluid filling ratio for each condenser type and the direct factors affecting the change of flow characteristics were analyzed. Series of experiments according to the input heat flux variation have shown that the change in the condenser type ultimately changes the subcooling amount at the inlet of the evaporator greatly. In particular, the use of the reflux condenser greatly reduced this subcooling and increased the overall thermosyphon circulating flow rate. Numerical modeling was also developed to predict the operating characteristics and circulation flow rate of the loop thermosyphon, and the model predictions were compared with experimental results with various conditions. Based on the experimental results of the two condensers, the error rate of the circulating flow rate prediction according to the supercooling amount change at the evaporator inlet was confirmed to be within 5 % prediction error.

Additional research has been conducted exploring the generation of electrical energy using the intrinsic instability of circulating flow in the thermosyphon. A flow triboelectricity generator consisting of a hydrophobic FEP tube and metal electrodes was installed at the condenser outlet of the loop thermosyphon to examine the possibility of electrical energy generation through friction between the working fluid flow and the FEP tube wall. Due to the instability of the thermosyphon flow, the fluctuation of the liquid column makes it possible to generate static electricity by continuous friction with the metal electrode. Electrode combinations were investigated by measuring the open circuit voltage according to the electrode arrangement of the triboelectric generator, exploring the electrical energy generation mechanism and generating the maximum voltage. The shape of the flow triboelectric generator optimized for the loop thermosyphon was investigated according to the thickness of the FEP tube insulator and the width of the electrode, and the charging performance of the electric energy from the optimized generator was greatly improved.

Contents

List of Figures	ii
Nomenclature	iv
1. Introduction	8
2. Effect of condenser type change on loop thermosyphon performance	
2.1. Loop thermosyphon design and numerical modeling	13
2.2. Condenser type	21
2.3. Loop thermosyphon experiment setup and method	22
2.4. Results and discussions	
2.4.1. Performance characteristics according to supply heat amount and FR	24
2.4.2. Flow visualization and $T_{\text{subcooling}}$ at evaporator	26
2.4.3. Analysis of condenser structural change	28
2.4.4. Comparison of modeling results and performance prediction	29
3. Loop thermosyphon flow instability	33
3.1. Triboelectric mechanism	35
3.2. Results and discussions	
3.2.1. Comparison of voltage characteristics according to mechanism	37
3.2.2. Comparison of open circuit voltage with wall thickness	40
3.2.3. Comparison of open circuit voltage with electrode width	41

3.2.4. Open circuit voltage results of optimized TEG	42
4. Conclusions and Future work	43
References	44

List of Figures

Figure 1. Schematic diagram for flow instability of loop thermosyphon	11
Figure 2. Schematic of loop thermosyphon	13
Figure 3. Numerical modeling diagram in loop thermosyphon	20
Figure 4. Condenser type applied to thermosyphon	21
Figure 5. Structure of loop thermosyphon and measurement locations	22
Figure 6. Performance characteristics according to heat amount and filling ratio change	24
Figure 7. Flowrate characteristics according to FR and heat amount with condenser type	25
Figure 8. Comparison of flow characteristics at evaporator outlet	26
Figure 9. Comparison of $T_{\text{subcooling}}$ at evaporator with condenser type	27
Figure 10. Analysis of performance change by condenser type	28
Figure 11. Comparison of thermosyphon modeling results and experimental Results at shell and tube condenser	29
Figure 12. comparison of thermosyphon modeling results and experimental results at trapezoid reflux condenser	30
Figure 13. Prediction of flowrate characteristics by $T_{\text{subcooling}}$ change	31
Figure 14. Loop thermosyphon flow instability	33
Figure 15. Triboelectric generator applied to thermosyphon and 3D modeling	34

Figure 16. Voltage generation process of triboelectric generator at top electrode	35
Figure 17. Voltage generation process of triboelectric generator at middle electrode	36
Figure 18. Voltage result according to mechanism	37
Figure 19. Peak to Peak voltage and V_{rms} result	38
Figure 20. FFT results for voltage generation	39
Figure 21. Voltage result according to insulator thickness difference	40
Figure 22. Voltage result according to electrode width	41
Figure 23. Optimized triboelectric generator characteristics	42

Nomenclature

<i>Symbol</i>		Unit
<i>A</i>	Area	$[m^2]$
<i>D</i>	Diameter of inner	$[m]$
<i>f</i>	Friction coefficient	$[-]$
<i>G</i>	Mass flux	$[kg/m^2 \cdot s]$
<i>g</i>	Gravity	$[m/s^2]$
<i>L</i>	Length	$[m]$
<i>H</i>	Height	$[m]$
<i>m</i>	Mass	$[kg]$
\dot{m}	Mass flow rate	$[kg/s]$
ΔP	Pressure drop	$[N/m^2]$
<i>Q</i>	Heat amount	$[W]$
<i>Re</i>	Renolds number	$[-]$
<i>V</i>	Velocity	$[m/s]$
<i>x</i>	Vapor quality	$[-]$
<i>Greek</i>		
<i>a</i>	Void fraction	$[-]$
ϕ^2	Two-phase multiplier	$[-]$
ρ	Density	$[kg/m^3]$
μ	Dynamic viscosity	$[Pa \cdot s]$

Subscript

<i>con</i>	Condenser
<i>eva</i>	Evaporator
<i>l</i>	Liquid phase
<i>v</i>	Vapor phase
<i>tp</i>	Two-phase

1. Introduction

The loop thermosyphon is an effective device to transfer the thermal energy between heat source and heat sink through phase-change of the working fluid. The loop thermosyphon can be divided into an evaporator part and a condenser part, where the working fluid in the loop thermosyphon turns into a vapor state by the heat input in the evaporator part and the vapor rises to the condenser part through the insulation part. The vapor condenses in condenser to the liquid state after heat exchange and finally returns to the evaporator by gravity. In principle, loop thermosyphon can be operated by gravity, but the evaporator section must be located below the gravitational field (compared to condenser). Loop thermosyphon is widely used as various applications, such as waste heat system, solar collector and electronic cooling by high thermal performance through the phase-change of the working fluid, stable operating conditions and simple structure [1], [2], [3], [4], [5].

Because the circulation of the working fluid in the loop thermosyphon is a very complex thermodynamic process, the temperature change of loop thermosyphon will result in the variations of the temperature, pressure and liquid or vapor distribution of the other components and eventually affect the overall thermal performance of the loop thermosyphon. For verification factor affecting the overall thermal performance of the loop thermosyphon, number of experimental investigations pertaining to the improvement of thermosyphon design and performance have been reported in years [6].

Singh et al [7] investigated heat input range of 50–300W and at various filling ratio (40%, 60% and 100%). It was found that filling ratio and heat input have a significant effect on the performance of the thermosyphon. Also, some researchers have investigated the performance of a thermosyphon using different working fluids like water, ethanol, methanol, acetone. Patel et al [8] and Pramod et al [9], experimentally, investigated performance of thermosyphon which the filling ratio was 50% with pure and binary fluids. The authors concluded that for pure acetone gives better thermal performance, and in the case of a binary mixture water-methanol gave the more performance. Also, the water charged thermosyphon was found to give a best thermal performance. Khandekar et al. [10] studied the overall thermal resistance of closed thermosyphon using pure water and various water based nanofluids as working fluids. They observed that all these nanofluids show inferior thermal performance than pure water since nucleation sites were closed by the deposition of the nanoparticles. Noie [11] experimentally analyzed the effects of the input heat transfer rates, the working fluid filling ratio, and the evaporator lengths (aspect ratios) on the heat transfer performance in closed thermosyphon. The filling ratio in his study was defined differently as the ratio of working fluid volume to the volume of the evaporator part.

For aspect ratios of 11.8, 9.8 and 7.45 the corresponding filling ratios for maximum heat transfer rate are 60%, 30% and 90%, respectively. Through previous research, operation characteristic and thermal performance of the loop thermosyphon is affected by several factors such as the type of working fluid, filling ratio (defined as the ratio of working fluid volume to condenser outlet vertical column), aspect ratio, operating pressure and length of various sections of the pipe [12]. Beside study on the operation characteristics and factors affecting thermal performance of thermosyphon, many previous studies have been conducted on condensers that are closely related to the performance characteristics of loop thermosyphon.

Condenser in thermosyphon play a role of making from the vapor phase-changed by the heat source into liquid through heat exchange with air or water. In this process latent heat is given up by the warm side process fluid and transferred to the cold side process fluid respectively ambient on the condenser [13]. Since the cooling method and type of condenser have a great influence on the operation characteristics and heat transfer performance of thermosyphon, many researchers have focused on the condenser design and study [14]. In the past few years there were realized several developments to improve the thermal effectiveness of condenser. New types of tube-side turbulence promoters and tube supports have been successfully introduced [15].

Rozzi et al. [16] examined the influence on heat transfer in a shell and tube heat exchanger using Newtonian/non-Newtonian fluids as the working fluids. Vicente et al. [17] carried out an experiment to study the heat transfer in corrugated tubes for laminar and turbulent flows using water and ethylene glycol as the working fluid. They observed that the corrugated tubes provide higher heat transfer and friction factor up to 30% and 25% than the smooth tube. Dong et al. [18] presented the heat transfer and friction factor characteristics in a spirally corrugated tube using water and oil as the working fluids. Their results revealed that the heat transfer coefficient and friction factor of the corrugated tube are higher than those of the smooth tube up to 120% and 160%, respectively. Laohalertdecha and Wongwises [19] performed an experimental work to examine the heat transfer coefficient and pressure drop in reflux condenser corrugated tubes by using R-134a as the working fluid. home et al. [20] put forward that the proper application of tubular heat transfer increase be able to reduce heat exchanger tubing linear footage by 25–75% compared with conventional plain tube units. Hosseini et al. [21] experimentally investigated the effect of different types of external tube surfaces on shell-side heat transfer coefficient and pressure drop of a shell and tube heat exchanger. The results showed that the performance of the heat exchanger greatly improved for micro-finned tubes at a higher reynolds number.

There are also a few researchers who have studied the effect of leakage flow on thermal performance of shell-and-tube heat exchangers. Roetzel and Lee [22] experimentally investigated the leakage flow in shell-and-tube heat exchangers with segmental baffles. They found that the shell-baffle leakage has great influence on the apparent overall heat transfer coefficient, which is based on the ideal plug flow model. Li and Kottke [23] performed experiments to determine the response of the pressure drop and local heat transfer on the shell-side of shell and tube heat exchanger to a change in the leakage between baffles and shell in the fully developed regime. They found that the leakage between baffles and shell can greatly reduce the pressure drop and the per-compartment average heat transfer coefficient.

Many previous studies on loop thermosyphon and condenser have focused on improving heat transfer and cooling the working fluid based on the type of working fluid, aspect ratio, filling rate, tube surface change, and so on. However, there is a lack of comparative studies on the effects of condenser types and structural differences on the loop thermosyphon and the consequences should be considered.

Therefore, the purpose of this study is to construct a laboratory-scale loop thermosyphon system and investigate and compare the performance characteristics of two self-manufactured condenser types. In addition, I examine the effect of the structural change of the condenser on loop thermosyphon and based on the experimental results, numerical modeling conducted the operating characteristics of loop thermosyphon under various conditions.

In the flow instability one of the characteristics of loop thermosyphon, I propose an energy harvesting method to harvest electrical energy using friction energy between working fluid and pipe at condenser outlet of loop thermosyphon.

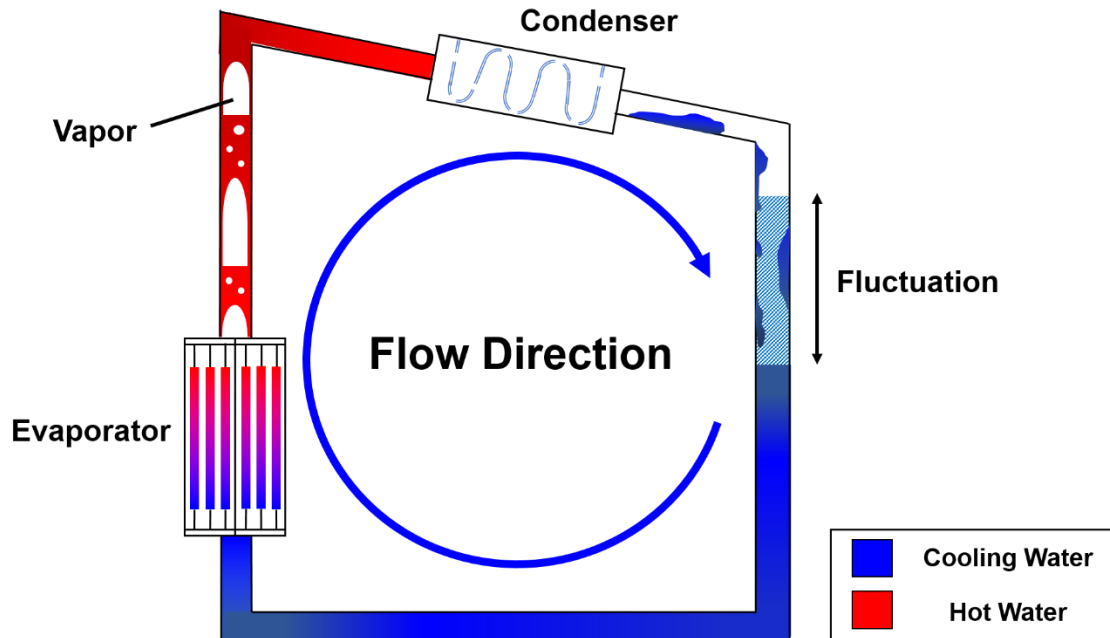


Figure 1. Schematic diagram for flow instability of loop thermosyphon

As mentioned earlier, when the evaporator is heated up the liquid starts boiling and vapor-liquid rises and condenses on the along the wall. Vapor-fluid also decrease pressure due to wall friction and indicate backflow phenomenon by gravity. This backflow of working fluid causes flow instability at condenser outlet of loop thermosyphon [24], [25].

Figure 1 is a schematic diagram showing the fluctuation at the condenser outlet according to the flow instability of the loop thermosyphon. Backflow phenomenon of working fluid by gravity at the evaporator mentioned above is very closely related to the fluctuation at condenser outlet of the loop thermosyphon. When backflow occurs, water column at condenser outlet has risen and decreased and continuous friction between the working fluid and the tube has been observed. These friction between the working fluid and the tube is contact electricity known as triboelectricity, which causes spontaneous charge generation on the two separated surfaces [26-29]. In other word, a phenomenon occurs in which an electric charge imbalance occurs due to friction between two objects and a spontaneous movement of free electrons is performed to recover an unbalanced electric potential difference [30-32]. In order to utilize the movement phenomenon of free electrons by friction between these two objects, a device called triboelectric generator has recently been attracting attention and energy generated from nature such as wind, heat and vibration of the surrounding environment harvesting and is converted into electrical energy, many studies are under way [30-37].

Based on this concept, I considered the triboelectric generator to effectively use up the friction energy consumed between the working fluid and the tube due to the flow instability at the condenser outlet of the loop thermosyphon. The triboelectric generator has the advantage of producing electrical output with high efficiency using cyclic contact and separation of two materials with different triboelectric polarities [38-40].

Until 2013, the triboelectric generator normally utilized two solid-phase polymers as contact materials because of their high Triboelectric polarity and concomitant high electrical output level. Therefore, a conventional triboelectric generator system works in a relatively dry environment to provide stable electrical output, because the presence of water would significantly suppress the solid–solid contact electrification phenomenon [39]. However, piezoelectric and triboelectric generator using such a solid–solid contact electrification phenomenon require a special dielectric and process are costly have durability problem due to abrasion caused by friction. Also, disadvantages to the problems of noise and external contamination and there is a problem that it is difficult to increase the efficiency because electricity is produced only in a specific direction [40].

To overcome the disadvantages of these solid-solid triboelectric generator, by using the concept that triboelectricity occurs when water contacts the polymer surface, a water-driven triboelectric generator utilizing solid–water contact electrification was first suggested by Wang's group in 2013 [41]. Given the nature of water, a water-driven triboelectric generator has several advantages, such as independence with humidity and robustness, compared to conventional triboelectric generator designed for contact among solid materials [41].

With reference to prior studies, application of polymeric polymer tubes at the condenser outlet in loop thermosyphon and showing the electrical energy generation in system units not previously studied using friction between the working fluid due to flow instability and the polymer. By applying a triboelectric generator which is limited to existing small-scale, units to the loop thermosyphon, it can show the high utilization potential of the triboelectric generator and shows many possibilities for producing alternative energy. In addition, I have determined the relationship between flow instability and electrical energy generation in the loop thermosyphon, measured the open circuit voltage according to the electrode arrangement and position, and then determined the characteristics.

the thermosyphon and the phase change of the working fluid for each part should be considered. Numerical modeling determined the pressure drop and the height of the water column at the condenser outlet based on the phase change of the working fluid and the mass preservation in each part. Based on the above analysis, the parameter model of the loop thermosyphon was established and the assumption is as follows.

- (1) Flow and heat transmission of the fluid are in a steady state.
- (2) All components are insulated from the outside.
- (3) All heat is supplied from the evaporator and all heat is released from the condenser.

In this numerical modeling, the working fluid was applied to the phase change process according to the quality change in each part. Part 1 and 2 reflect the pressure drop based on the single phase because the working fluid is liquid after heat exchange in the condenser and Part 3 and 5 show the phase change process of the evaporator and condenser according to the quality change. As a result, the pressure drop of the single phase and the two phases was reflected and the Part 4 was applied to the two-phase pressure drop without changing the quality assuming that it was a complete insulation from the outside. In Part 5, the height of the water column at the condenser outlet was obtained based on the mass change of the working fluid generated in each part, and the reliability of the modeling was shown through the difference of the total pressure drop in each part and the pressure drop according to the water column change.

Part 1 and 2 : Bottom – Evaporator inlet (Single Phase)

As mentioned above, the working fluid flowing through thermosyphon can be divided into single phase and two-phase flows according to phase change, and the pressure drop process of each part is also applied differently. In Parts 1 and 2 are three in total, resulting in a 90° bend friction pressure drop at both end of the pipe and friction drop and an expansion-reduction friction pressure drop in the coriolis flowmeter. The single-phase flow friction pressure drop and bend friction pressure drop can be calculated from classical fluid flow such as Fox et al. (1999) and Chisholm the B-type equation (1980) [42]. In this study, modified the pressure drop equation as a function of mass flowrate.

$$\Delta P_f = f_b \cdot \frac{\rho}{2} \cdot \left[\frac{\dot{m}}{\rho \cdot A_c} \right]^2 \cdot \frac{L_b}{D} \quad (1)$$

where x/d equivalent length, used the value of 12

$$\Delta P_b = f_b \cdot 12 \cdot \frac{\left[\frac{\dot{m}}{\rho \cdot A_c} \right]^2}{2 \cdot \rho} \quad (2)$$

For smooth pipes laminar flow and turbulent flow, friction coefficient f_b can be computed as

$$f_b = \frac{64}{Re} \quad (\text{for laminar flow}) \quad (3)$$

$$f_b = 0.3164 \cdot Re^{-0.25} \quad (\text{for turbulent flow}) \quad (4)$$

Where, Re is the Reynolds number and is defined as

$$Re = \frac{\rho \cdot V \cdot D}{\mu} \quad (5)$$

The pressure drop in parts 1 and 2 is determined by the initial values and changed through iteration. The pressure drop generated in the flowmeter are calculated as follows as and the loss coefficient K is reflected as 0.24 according to the expansion-reduction pipe area ratio of Borda-Carnot [43].

$$\Delta P_{flowmeter} = (f_b \cdot \frac{L_{flowmeter}}{D} + 0.24) \cdot \frac{\rho \cdot V^2}{2 \cdot g} \quad (6)$$

Part 3 and 5 : Evaporator and Condenser (Two Phase)

Part 3 shows pressure drop in evaporator and working fluid is phased from liquid to vapor. The two-phase condition of the working fluid was set according to the quality and the single phase and two-phase pressure drop equation were divided according to the phase change of the working fluid. In the case of the single phase, the pipe friction drop mentioned in Part 1 and 2 was used and the pressure drop is added due to the vertical tube of the evaporator to the reverse direction of gravity.

$$\Delta P_g = \rho \cdot g \cdot L_{eva} \quad (7)$$

C_p is derived by temperature and pressure and according to the thermal energy equation, the temperature on the single-phase can be defined as follows.

$$T_{eva,j} = \frac{Q}{\dot{m} \cdot C_p} + T_{eva,j-1} \quad (8)$$

When the temperature at the single phase is equal to the saturation temperature at the evaporator pressure, it is considered as the two-phase state and the calculation is proceeded according to the initial set $x(\text{quality}) = 0.001$. In the two phase state, the pressure gradient of the evaporator consists of three parts : friction, gravity, and acceleration.

The pressure gradients are indicated by the following subscripts $f.two$, $g.two$ and $a.two$.

$$\Delta P = \Delta P_{f.two} + \Delta P_{g.two} + \Delta P_{a.two} \quad (9)$$

The two phase friction pressure drop was modeled using the Homogeneous model (HEM) [44].

$$\Delta P_{f.two} = \frac{2}{D} \cdot f_{tp} \cdot (G)^2 \cdot (v_f + x \cdot v_{fg}) \quad (10)$$

Where, G is the mass flux.

$$G = \frac{\dot{m}}{A_c} \quad (11)$$

The friction coefficient for turbulent flow is computed as

$$f_{tp} = C_{fre} \cdot \left[\frac{G \cdot d}{\mu_{Mc}} \right]^{-S} \quad (C_{fre} = 0.079, S = 0.25) \quad (12)$$

Where, two-phase viscosity was applied to McAdams model [45].

$$\mu_{Mc} = \frac{\mu_v}{x} + \frac{\mu_l}{1-x} \quad (13)$$

Pressure drop by two phase gravity is shown as follows

$$\Delta P_{g.two} = \rho_m \cdot g \cdot L_{eva} \quad (14)$$

Where, ρ_m is a two phase mixture density, which depends on the void fraction,

$$\rho_m = \rho_l \cdot (1 - \alpha) + \rho_g \cdot \alpha \quad (15)$$

The void fraction of two-phase was calculated using the Zivi void fraction model [46].

$$\alpha = \frac{1}{1 + \left[\frac{1-x}{x} \right] + \left[\frac{\rho_g}{\rho_l} \right]^{\left(\frac{2}{3} \right)}} \quad (16)$$

The change in quality is as follows and the enthalpy vaporization can be derived as the saturation

temperature according to the pressure change.

$$x_j = \frac{Q}{\dot{m} \cdot h_{fg}} + x_{j-1} \quad (17)$$

Acceleration pressure drops are caused the velocity change by changes in the quality and void fraction and it is defined as

$$\Delta P_{a.two} = G^2 \cdot v_{fg} \cdot qflux \cdot \left[\frac{D}{\dot{m} \cdot h_{fg}} \right] \quad (18)$$

In the case of a condenser of Part 5, it is assumed that the pressure drop in evaporator is reversed and all heat escape to the condenser. Calculation is performed to single phase from two phase and the quality of the condenser exit is always assumed to be zero.

Part 4 : Rising tube – Condenser inlet (Two Phase)

This numerical modeling has not changed quality since it assumed that there is no heat loss from the outside. Therefore, the pressure gradient of Part 4 is as follows and a two phase bend pressure drop is added.

$$\Delta P = \Delta P_{f.two} + \Delta P_{g.two} + \Delta P_{b.two} \quad (19)$$

The friction pressure drop equation in this part applied to Müller-Steinhagen and HeckCorrelation, a Separate Flow Model [47].

$$\Delta P_{f.two} = \Delta P_{f.l} + 2 \cdot x \cdot (\Delta P_{f.l} - \Delta P_{f.v}) \left[(1-x)^{\frac{1}{3}} + \Delta P_{f.v} \cdot x^3 \cdot L_{rising} \right] \quad (20)$$

Where, $\Delta P_{f.l}$ and $\Delta P_{f.v}$ are expressed as single-phase friction pressure drops of only liquid and vapor, respectively,

$$\Delta P_{f.l} = f_l \cdot 2 \cdot \frac{\left[\frac{\dot{m}}{Ac} \right]^2}{\rho_l \cdot D} \quad (21)$$

$$\Delta P_{f.v} = f_v \cdot 2 \cdot \frac{\left[\frac{\dot{m}}{Ac} \right]^2}{\rho_v \cdot D} \quad (22)$$

The friction factors and reynolds numbers for liquid ($k = l$) and vapor ($k = v$) are expressed as

$$f_k = \frac{16}{Re_k}, \quad Re_k < 2,300 \quad (23)$$

$$f_k = \frac{0.079}{Re_k^{0.25}}, \quad 2300 < Re_k < 20,000 \quad (24)$$

$$f_k = \frac{0.046}{Re_k^{0.2}}, \quad Re_k > 20,000 \quad (25)$$

Pressure drop acting in the opposite direction of gravity is applied identically to the Part 3 equation. The two-phase bend pressure drop was changed to a function for mass flow rate by referring to Chisholm the B-type equation (1980).

where x/d equivalent length, used the value of 12

$$\Delta P_{b.two} = f_{b.two} \cdot 12 \cdot \frac{\left[\frac{\dot{m}}{A_c}\right]^2}{2 \cdot \rho \cdot D} \cdot \Phi^2 \quad (26)$$

The definition of two-phase multiplier is as follows

$$\Phi^2 = 1 + \left(\frac{\rho_l}{\rho_v} - 1\right) \cdot (multi_b \cdot x \cdot (1 - x) + x) \quad (27)$$

Where, r/d ratio of bend and tube diameter used value 2

$$multi_b = 1 + \left(\frac{2.2}{f_{b.two} \cdot \frac{x}{d} \cdot \left(2 + \frac{r}{d}\right)} \right) \quad (28)$$

The friction loss coefficient was expressed as a function of friction pressure drop in single-phase liquid and vapor.

$$f_{b.two} = \Delta P_{f.l} \cdot (1 - x) + \Delta P_{f.v} \cdot x \quad (29)$$

Part 6 : Water Column

The part after condenser predicts the characteristics of thermosyphon using the difference of the sum of all previous part pressure drop and pressure according to water column change. H_{sys} shows the length of the vertical pillar of the condenser exit and the filling ratio(FR) shows as the ratio of the length of water column about the H_{sys} length

$$H_{initial} = H_{sys} \cdot FR \quad (30)$$

Before the operation of thermosyphon, the initial mass of the entire working fluid can be obtained as follows:

$$m_{initial} = 2 \cdot \rho \cdot A_c \cdot H_{initial} + \rho \cdot L_b \cdot A_c \quad (31)$$

The mass variation of liquid by phase change in evaporator, rising tube, and condenser can be defined as follows through mass conservation.

$$m_{liquid} = m_{initial} - m_{eva} - m_{rising} - m_{con} \quad (32)$$

The mass variations according to the phase change in the evaporator, the rising tube, and the condenser were defined as follows.

$$m_{eva} = \rho_l \cdot L_{eva} \cdot A_c + \rho_v \cdot L_{eva} \cdot A_c \quad (33)$$

$$m_{rising} = \rho \cdot (1 - \alpha) \cdot A_c \cdot L_{rising} + \rho \cdot \alpha \cdot A_c \cdot L_{rising} \quad (34)$$

$$m_{con} = m_{eva} \cdot \frac{L_{con}}{L_{eva}} \quad (35)$$

The water column changes according to the mass change of the liquid are defined as follows.

$$H_{operation} = \frac{m_{initial} - \rho \cdot A_c \cdot L_b}{\rho \cdot A_c} \quad (36)$$

The pressures drop following the water column changes were defined as follows.

$$\Delta P_{head} = \rho \cdot g \cdot (H_{initial} - H_{operation}) \quad (37)$$

Finally, modeling is completed based on the difference of pressure drop by the water column and the pressure drop occurring in all parts, and the mass flow of each part is calculated as a variable.

$$\Delta P_{total} - \Delta P_{head} \quad (38)$$

In this modeling, the error range of the difference between the two pressures is about 0.6%, which shows high reliability.

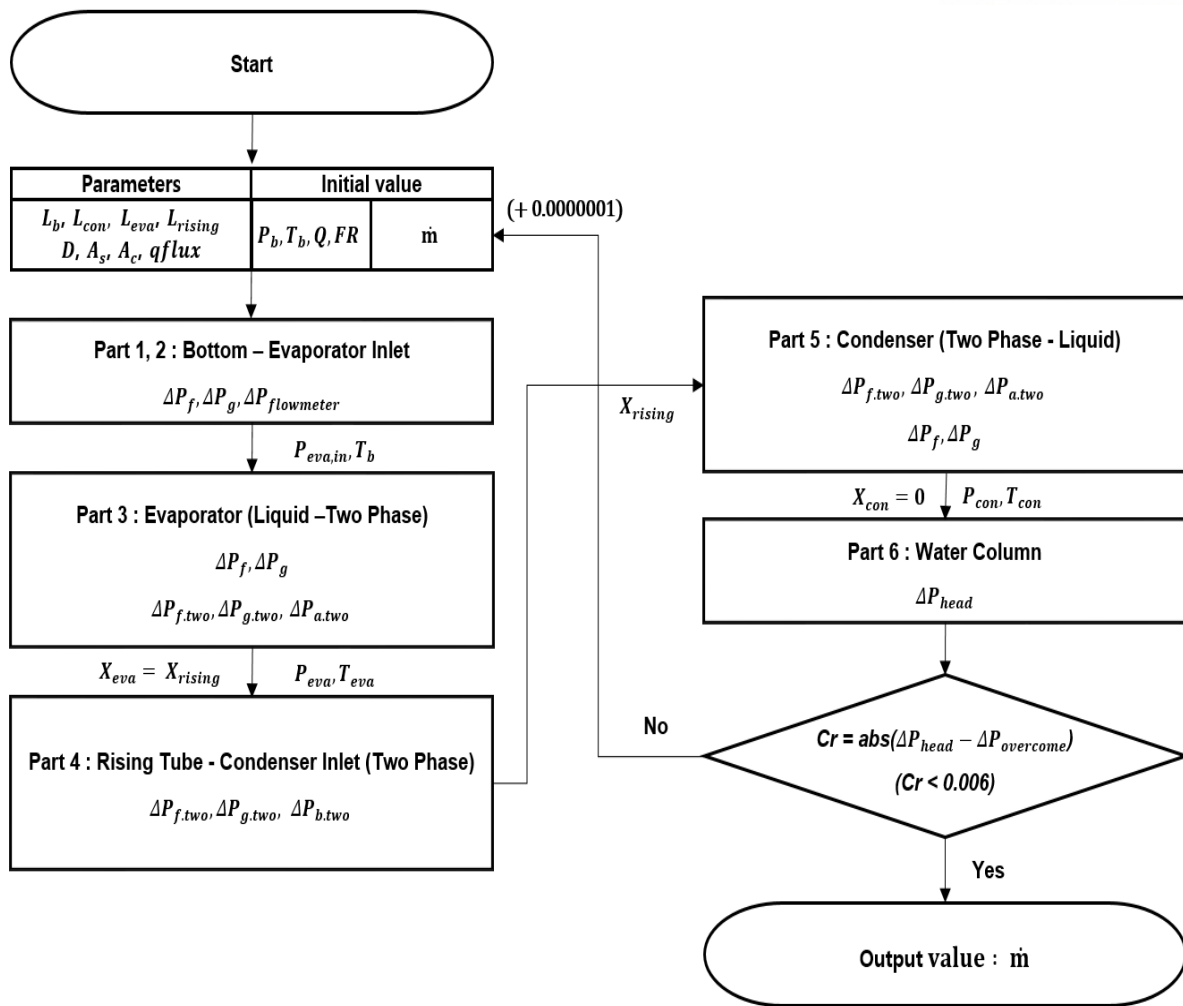


Figure 3. Numerical modeling diagram in loop thermosyphon

The detailed system-solving flowchart is presented in Figure 3 and used the software Engineering Equation Solver. To start the calculation, the initial values such as P_b , T_b , Q , FR and \dot{m} are specified based on the experimental values. Then, the difference of pressure drop according to the pressure drop and water column change of each part is repeatedly calculated by varying the \dot{m} until it reaches the specified range.

2.2. Condenser type

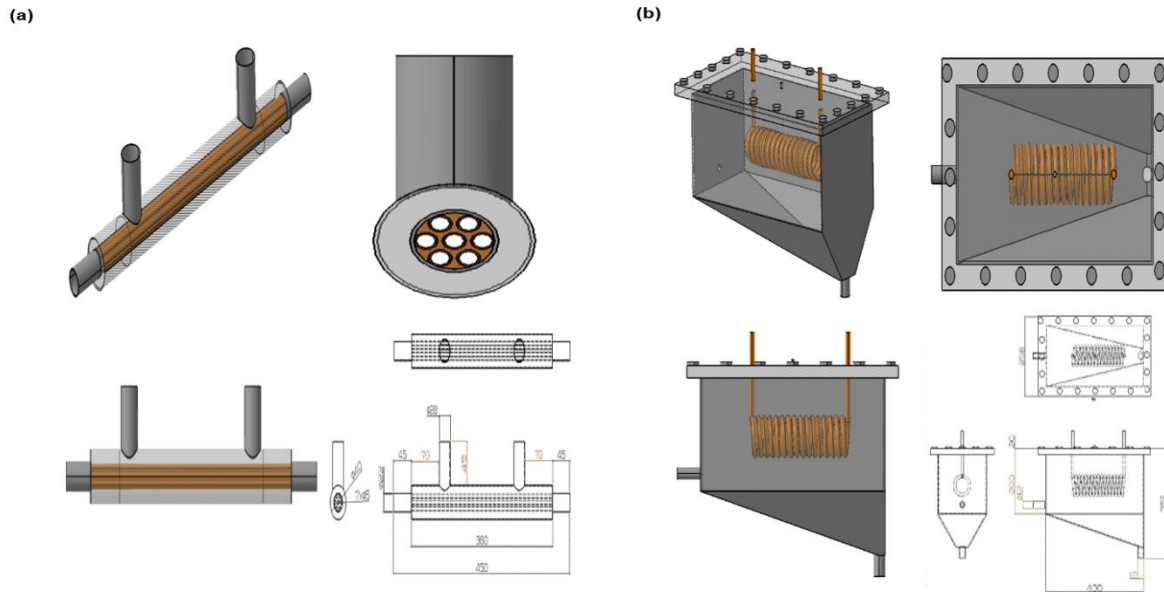


Figure 4. Condenser type applied to thermosyphon

Figure 4 (a), (b) is two types of condenser used in this study. Figure 4 (a) is a condenser of shell and tube type, in which working fluid flows into a stainless tube with a length of 360 mm and a diameter of 40 mm and seven copper tubes with a diameter of 5 mm are divided. Through the copper pipe, the working fluid is divided after entering and the condensation process occurs according to the length. There are two tubes with a diameter of 28 mm and a length of 45 mm outside the condenser, which will allow coolant to flow in and exit after convection heat exchange with working fluid.

Figure 4 (b) is a stainless trapezoid reflux condenser with a length of 400mm and a width of 230 mm, with a copper coil of 3.175 mm outer diameter and 1 mm thick in the center of the condenser. The copper coil is a pipe through which coolant flow and the working fluid entering into the condenser and the working fluid condensed after convection heat exchange are dropped by gravity. then, it flows according to the tilted shape and circulated in loop thermosyphon.

In this study, the flowrate and operation characteristics of loop thermosyphon according to condenser change were compared as variables by the heat amount and the filling ratio.

2.3. Loop thermosyphon experiment setup and method

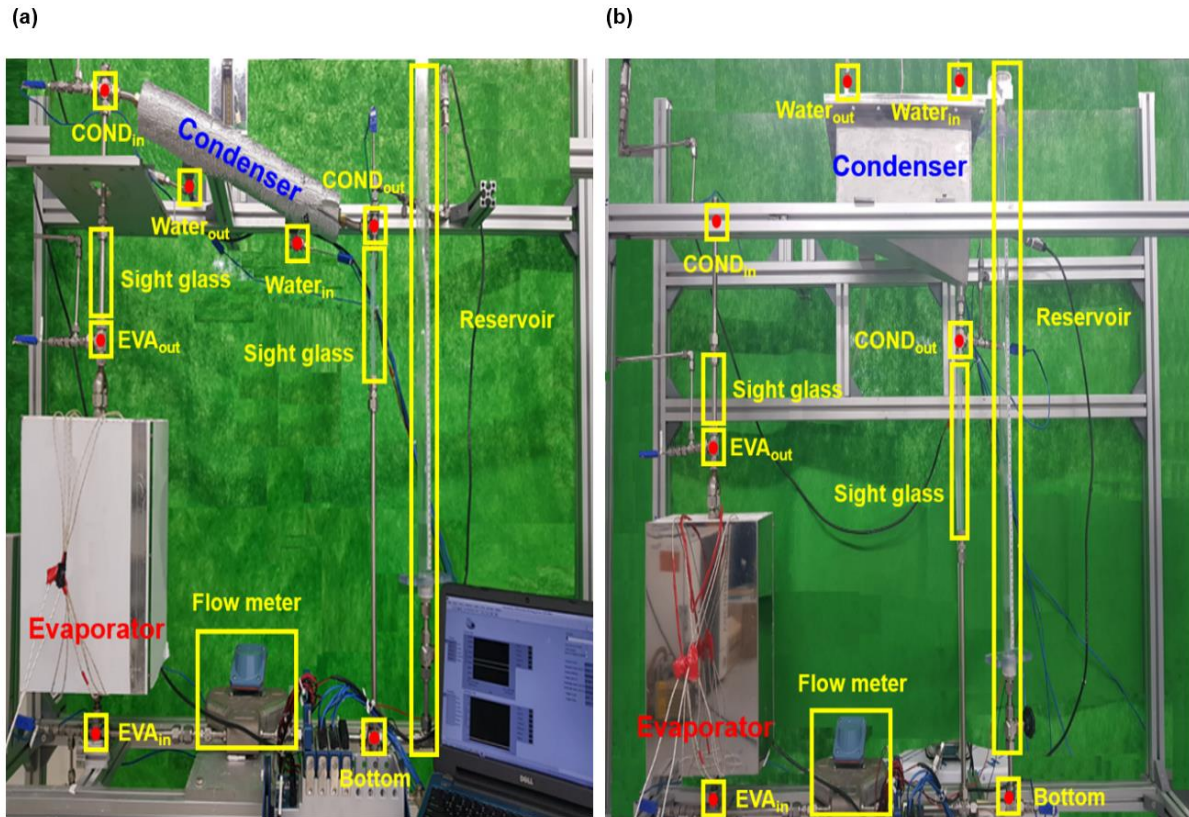


Figure 5. Structure of loop thermosyphon and measurement locations

Figure 5 (a), (b) shows the experiment device of loop thermosyphon according to the condenser change above mentioned. The connected pipes of loop thermosyphon were fabricated using stainless steel pipes with a diameter of 12.7mm and a thickness of 2mm and the working fluid is DI water. It consists of an evaporator, a condenser, and a water bath for coolant supply. The evaporator of thermosyphon consists of a copper plate heater of 120mm x 215mm x 30mm and the bolts are fastened to both sides of each plate to fix outside of the copper pipe and the ceramic insulation is added around the evaporator for insulation from the outside. The heater was powered by a variable transformer and the power was measured using a multimeter. The water bath for supplying coolant to condenser was connected to flowmeter to control the supply flowrate and in this experiment, the same supply flow rate of 20ml/min was carried out.

To measure the pressure, temperature and flowrate changes by the phase change that occurs when the working fluid circulates in thermosyphon, five pressure transducers and seven T-type thermocouples were inserted into each part of the stainless pipe and the flowrate is measured when the working fluid passes through the coriolis flowmeter in the horizontal tubes of thermosyphon.

The measured position was set up with a pressure transducer and a thermocouple at the inlet and outlet of the evaporator, condenser, and coolant and flowmeter was installed at the center of the horizontal tube of the thermosyphon and it was marked as a red point of Figure 5 (a), (b). For data collection of the measurement location, recorded it using DAQ system and labview of national instruments

After loop thermosyphon was designed, leakage test was performed before start experiment and the loop thermosyphon was filled with high pressure nitrogen gas and the pressure was adjusted by a double gauge high pressure piston controller and all valves connected to the outside were locked. The system was left intact for 24 hours and the change in pressure gauge was observed through labview and the change in pressure was not recorded for 24 hours. Finally, the leakage test was successfully completed and after valve open nitrogen gas in the thermosyphon removed.

The experiment of loop thermosyphon according to condenser change was carried out under the same conditions and the experiment method opened the valve connected to reservoir and supplied DI water, which is the working fluid, through the upper inlet part of reservoir. Then, the height of the working fluids in exit vertical stainless tube of the condenser of thermosyphon and the level of the reservoir match the filling ratio. after the valve in which reservoir and thermosyphon are connected is closed and after pressure with outside is secluded and then activate the water bath for coolant supply to the condenser. The supplied coolant flowrate is controlled through the flowmeter. Finally, the power meter is operated to supply heat source to the evaporator to operate the evaporator composed of six electric strip heaters and the minimum heat input used in this experiment was 200W and the maximum heat input was 600W. The temperature and pressure of the measurement location were considered to steady state when the temperature and pressure of the measurement location were constant over time and this procedure was repeated in various thermal input ranges for the reliability of the experiment.

2.4. Results and discussions

2.4.1. Comparison of operation characteristics according to condenser

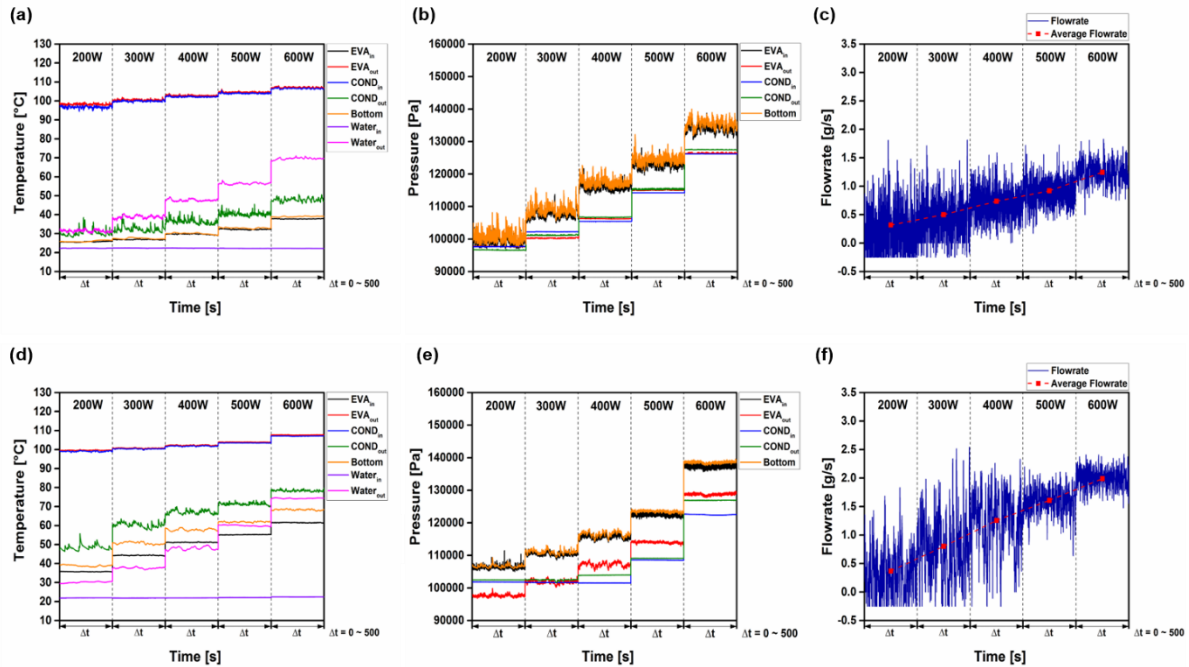


Figure 6. Characteristics of pressure, temperature and flowrate with condenser type

I compared the operation characteristics of the two condensers applied to the loop thermosyphon mentioned above according to supply heat amount and both cases were subjected to the same coolant flowrate at FR 70 and steady state 500 second. Figure 6 (a), (b) and (c) show the temperature and pressure of the loop thermosyphon in the shell and tube condenser and (d), (e) and (f) show the trapezoid reflux condenser.

both cases showed increased pressure, temperature and flowrate due to increased evaporation and condensation of working fluids as the heat amount increased. In addition, the biggest difference between the two results was the $COND_{out}$ temperature and flowrate higher in the trapezoid reflux condenser than shell and tube condenser. The $COND_{out}$ temperature of the trapezoid reflux condenser was measured at temperature of 13 ~ 30 °C higher than the shell and tube condenser under all heat mount conditions.

The increase in the $COND_{out}$ can be seen as an increase in the flowrate because the working fluid requires less time to evaporate even if the same heat amount is supplied from the evaporator.

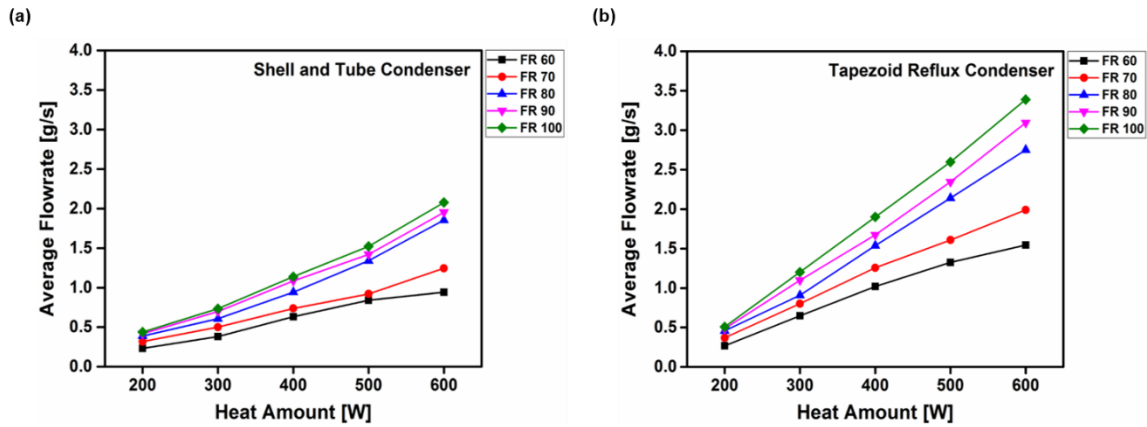


Figure 7. Flowrate characteristics according to FR and heat amount with condenser type

It can be seen that the change of $COND_{out}$ due to the difference of condenser mentioned above has a great influence on the flowrate characteristic results. To confirm the change in the flowrate characteristics with these condenser differences, the results were compared under the heat amount and FR conditions. Figure 7 (a) and (b) show the result of comparing the flowrate characteristics at the heat amount and the FR condition according to the difference of the condenser.

When comparing the two results, the flowrate characteristics of the trapezoid reflux condenser show very high results under all conditions, with a difference of about 0.2 to 1.5 g/s. In particular, the difference in flowrate characteristics between the two condensers does not vary significantly with changes in FR at low heat amount but becomes more apparent as the heat amount increases. This is because as the heat amount increases, the evaporation amount of the working fluid increases, and the temperature of the $COND_{out}$ is further increased. Accordingly, the temperature of the working fluid flowing into the evaporator becomes higher and the circulating flowrate of the loop thermosyphon is greatly influenced.

2.4.2. Flow visualization comparison at evaporator and condenser outlet

The difference in the $COND_{out}$ due to the condenser change mentioned above causes a difference in temperature of the working fluid flowing into the evaporator, resulting in a difference in evaporation amount at the evaporator. To understand the affection of evaporator due to the change of these condenser outlet temperature, flow pattern was compared through the sight glass tube at the evaporator outlet. The flow pattern visualization was photographed with 1000 frames per second using a high-speed camera and for accuracy, repeatedly was performed.

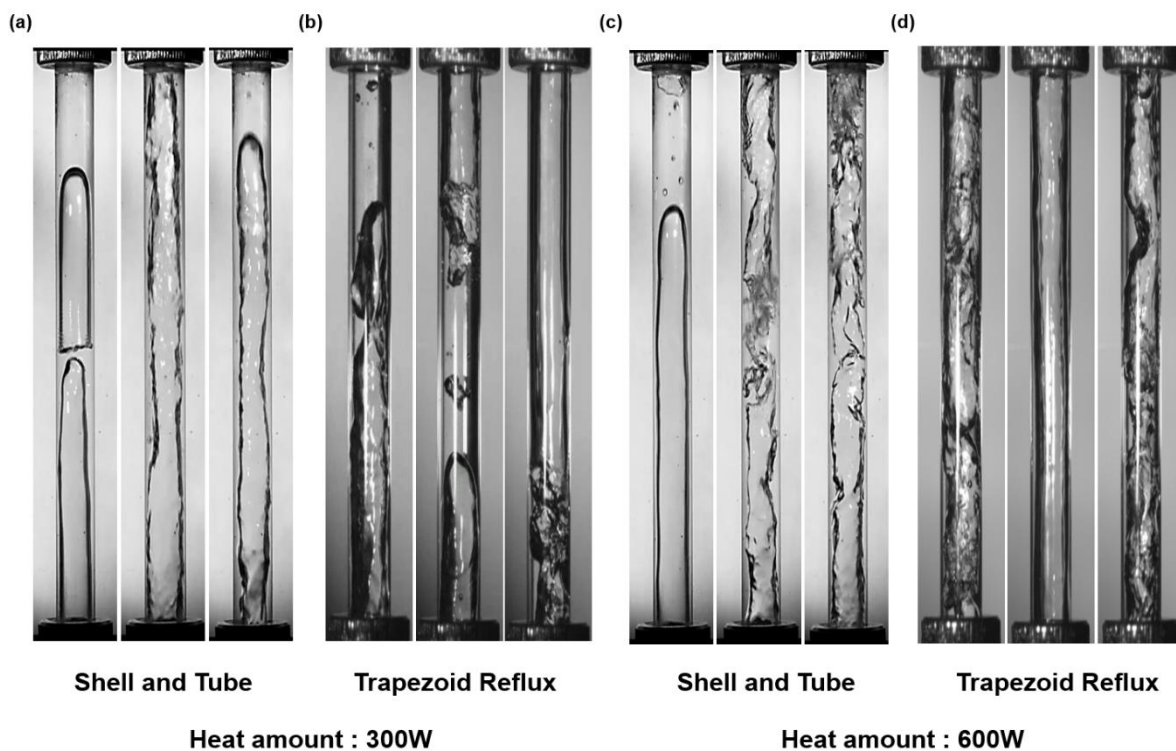


Figure 8. Comparison of flow characteristics at evaporator outlet

Figure 8 (a), (b), (c), (d) shows the flow pattern characteristics at the evaporator outlet of shell and tube condenser and trapezoid reflux condenser in FR 70, 300W, 600W as experimental conditions.

At Figure 8. (a), (c), show long slug flow patterns, which do not change over time. The slug flow decreased along the stainless tube due to the condensation according to length and resulting in a backflow phenomenon due to effect of gravity due to increase of density. This rising in the slug flow occurs more frequently as the heat amount increases, and the backflow and rising of the working fluid coexist. However, in Fig. 8 (b) and (d), a flow pattern showing a different kind of high quality was observed and the evaporation frequency also greatly increased. Due to the increase of the evaporation frequency, evaporation was influence more rising of working fluid between backflow and rising of the working fluid.

In general, the flowrate characteristics exhibit flow pattern of low quality as the flowrate increases but exhibit high quality characteristics in actual flow visualization. The result is that the temperature of the working fluid flowing into the evaporator increases due to the change of the condenser outlet temperature due to the condenser change mentioned above and the difference in evaporation amount at the same amount of supplied heat is generated.

Therefore, the evaporation amount is increased and the circulating flowrate characteristics of the loop thermosyphon are greatly increased.

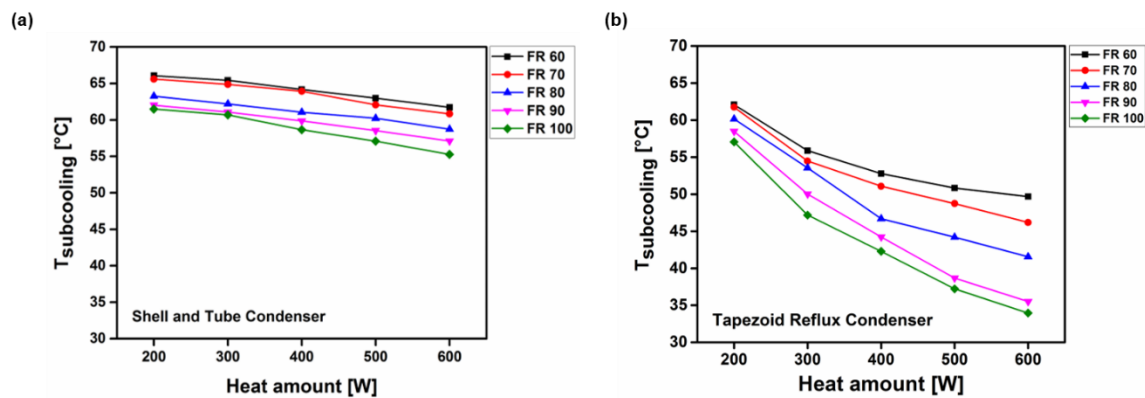


Figure 9. Comparison of $T_{subcooling}$ at evaporator with condenser type

The temperature of the working fluid entering the evaporator due to the condenser change has a significant effect on the circulating flowrate of the loop thermosyphon. To confirm this effect, the $T_{subcooling}$ of the evaporator according to condenser change was compared and the $T_{subcooling}$ was defined as the value obtained by subtracting the temperature of the working fluid entering from the saturation temperature of the working fluid in evaporator.

Figure 9 (a) and (b) show the change in $T_{subcooling}$ due to FR and heat amount changes in two condensers. Comparing the two results, the trapezoid reflux condenser showed lower $T_{subcooling}$ results in all sections than the shell and tube condenser.

At 200W, the $T_{subcooling}$ of the two condensers shows a difference of about 5°C and at 600W shows a difference of up to 20°C. The difference the flowrate characteristics and the $T_{subcooling}$ of the two condensers was small in low heat amount, but the difference of flowrate characteristics and the $T_{subcooling}$ was found to be larger as heat amount increased.

Therefore, it can be seen that change of the evaporator $T_{subcooling}$ due to the change of the condenser greatly influences the circulating flowrate characteristics of the loop thermosyphon.

2.4.3. Analysis of condenser structural difference

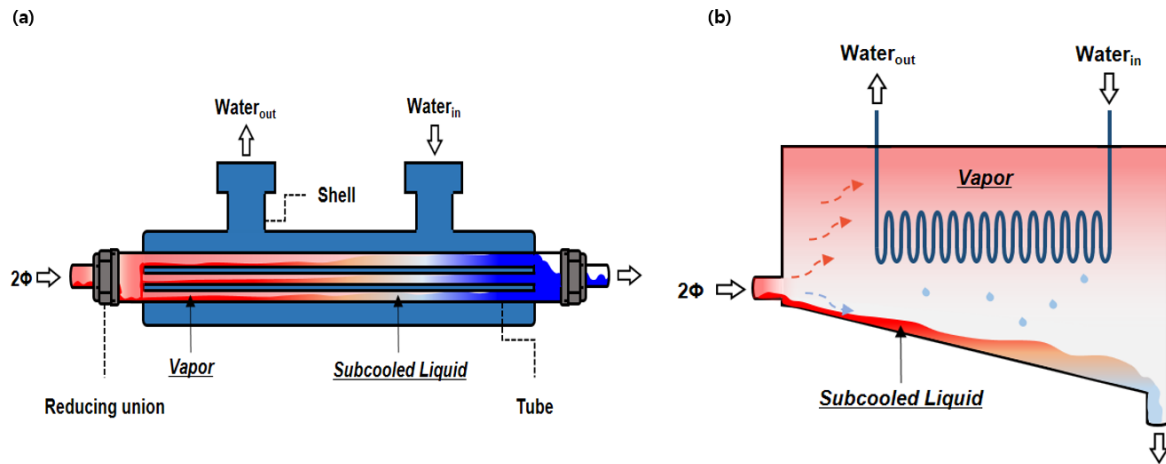


Figure 10. Analysis of performance change by condenser type

The change of the flowrate characteristic of loop thermosyphon is associated with the $T_{\text{subcooling}}$ of the evaporator, which is related to the condensation mechanism of the working fluid by structural difference of the condenser. To explain the condensation mechanism each condenser, the Figure 10 (a) shows condensation mechanism of working fluid in shell and tube condenser and the Figure 10 (b) trapezoid reflux condenser.

In the case of shell and tube condenser, the evaporated vapor and a small amount of liquid come into the seven tubes in the condenser mentioned above. The coolant then flows through the two tubes on the outside of the condenser and the steam and a small amount of liquid are phase-changed and cooled to liquid through convection heat exchange with coolant. In addition, the shell and tube condenser can be seen to have additional cooling along the length by the coolant even after condensation.

On the other hand, the trapezoid reflux condenser has a coil with a flowing coolant in the center of the condenser and the vapor with low density moves to the space above the condenser, condenses after convection heat exchange and falls downward by gravity. Subsequently, condensed liquid fallen by gravity flows along the inclined side. The biggest difference between these two condensers is the occurrence with coolant of additional cooling of condensed liquids.

For shell and tube condenser, the condenser outlet temperature is low because the condensed fluid causes additional cooling depending on the coolant and length. On the other hand, the trapezoid reflux condenser has a relatively high temperature at the condenser outlet because the condensed fluid only generates cooling according to the length, which results in a low of $T_{\text{subcooling}}$ at the evaporator.

Therefore, the structural difference of the condenser causes the $T_{\text{subcooling}}$ change in evaporator and the evaporation is more frequent even if the same heat amount is supplied from the evaporator, so the flowrate characteristics are increase.

2.4.4. Comparison of modeling results and performance prediction

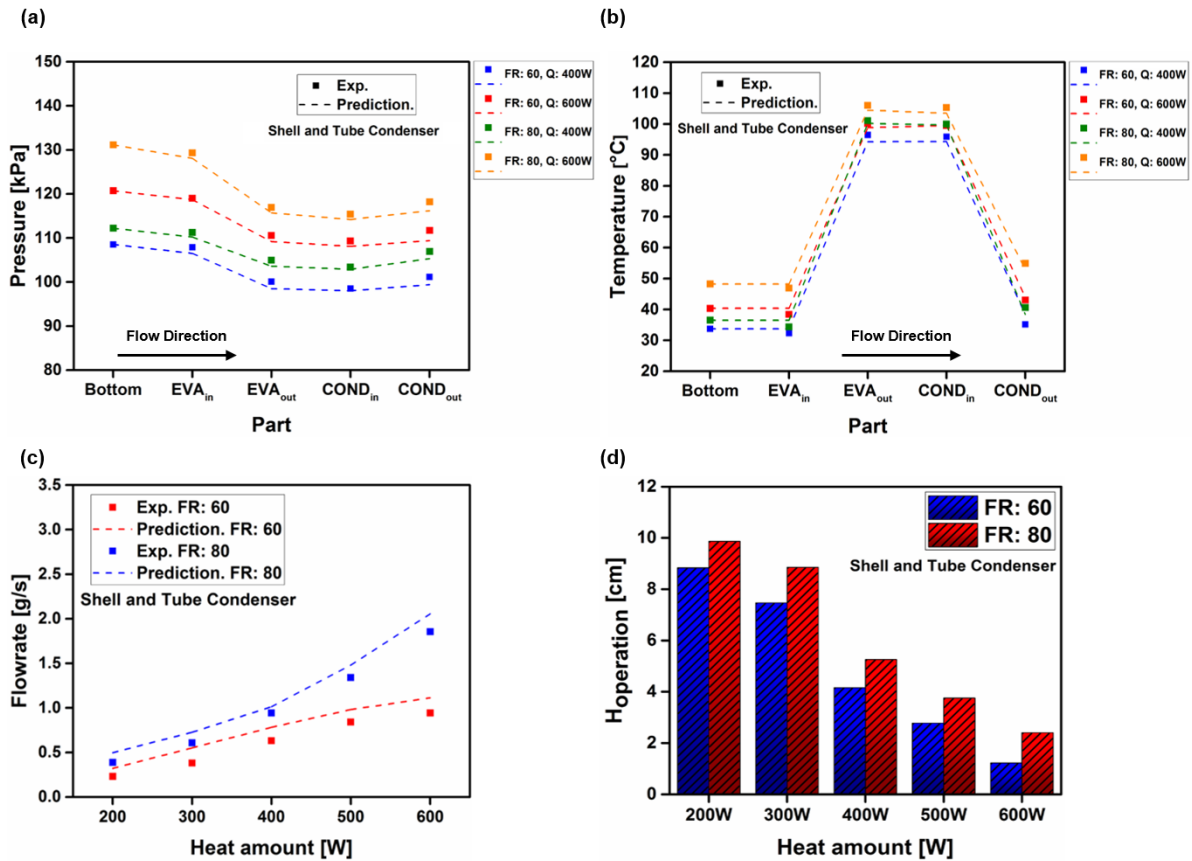


Figure 4. Comparison of thermosyphon modeling results and experimental results at shell and tube condenser

Based on the experimental results of loop thermosyphon due to condenser change, we propose a method to predict the performance of thermosyphon through Numerical modeling described above. Based on the initial value at Bottom, the pressure, temperature and flow rate of each section according flowrate change were compared with the actual data.

Figure 11 (a) and (b) represent the calculation result of the pressure and temperature in each part of shell and tube condenser through modeling. When compared with the actual experimental results according to the heat amount and FR showed similar tendency, and both results showed a rapid pressure drop in the evaporator. This indicates that the pressure drop by friction, gravity, and acceleration in the two phase is dominant.

In the modeling described above, the equation of all pressure drops was modified for the flowrate, which is a variable condition, and the experimental results were compared in Figure 11 (c), which is the modeling result. However, the modeling results may differ slightly from the experimental results because the measured mean value is used.

In the actual experiment, the water column at condenser outlet change decreased as the heat amount increased and the water column increased according to the FR change, which showed the same tendency in modeling in Figure 11 (d).

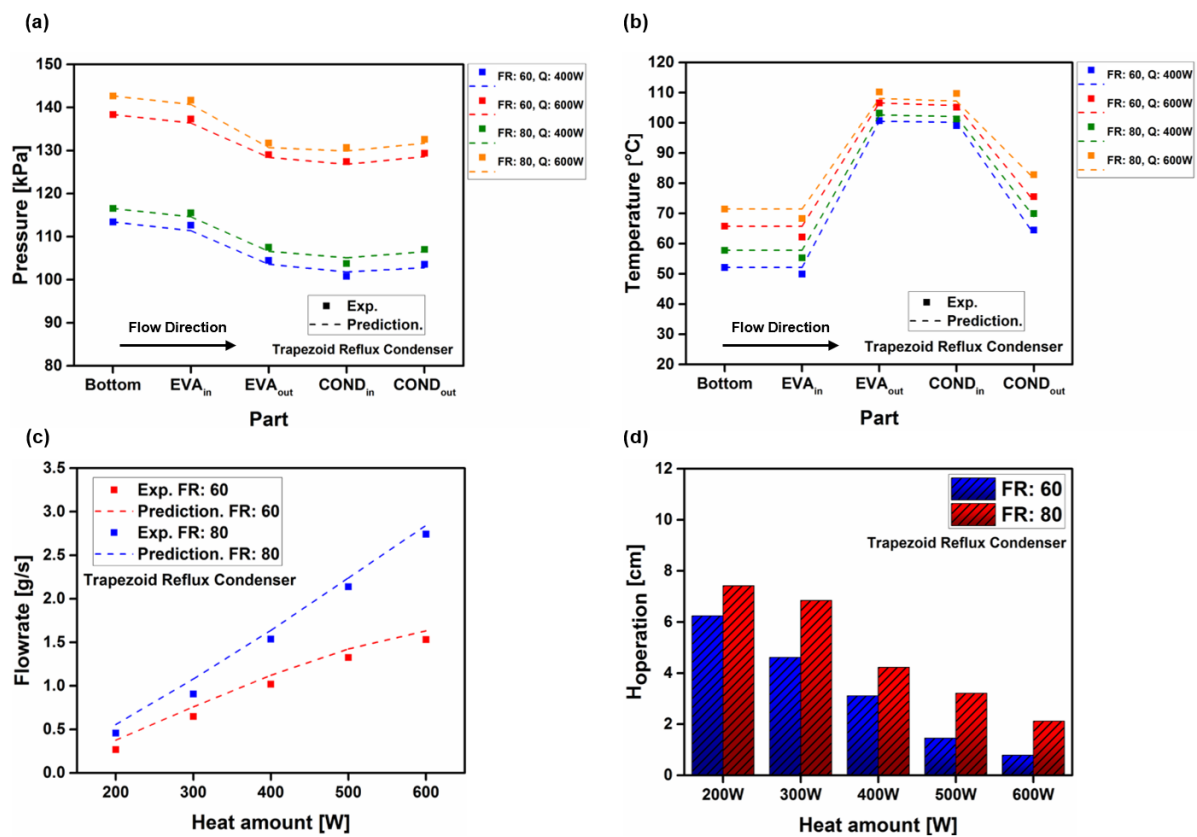


Figure 5. Comparison of thermosyphon modeling results and experimental results at trapezoid reflux condenser

Based on the results of the thermosyphon experiment according to the condenser change, I compared the results to confirm the same tendency in this modeling. The experimental results and the modeling results were compared under the same conditions applied to the shell and tube condenser, and the experimental and modeling results of the trapezoid reflux type showed the same tendency. In Figure 12 (a), (b) and (c) show the result of pressure and temperature, flowrate, the error is about 5%, similar to the shell and tube condenser. In addition, the height difference of the water column according to the condenser change shown in Figure 12 (d) was also similar to the modeling results and the lower result than the shell and tube condenser also showed the same tendency.

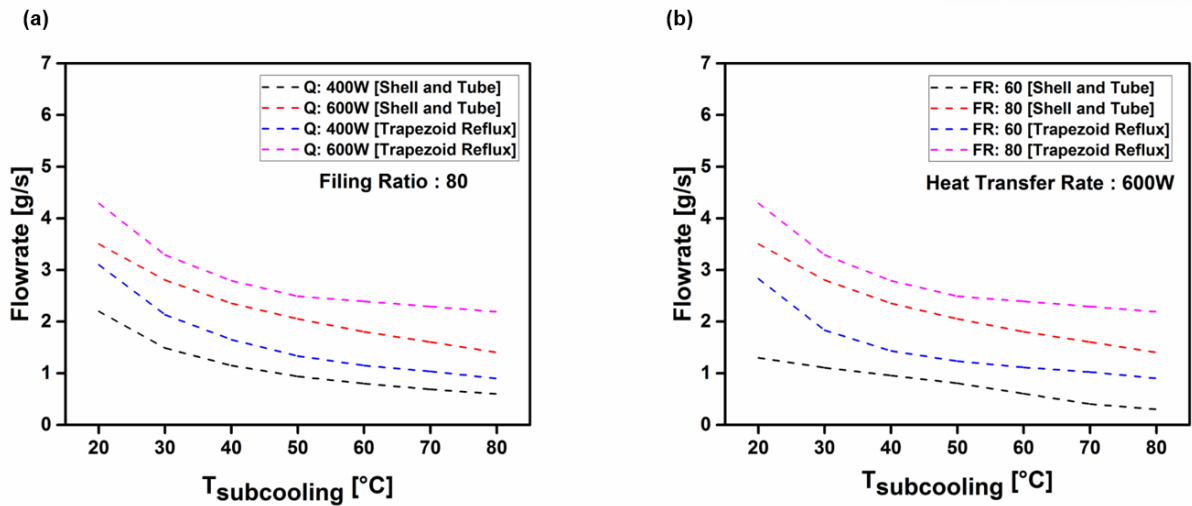


Figure 13. Prediction of flowrate characteristics by $T_{\text{subcooling}}$ change

This study found that the supercooling difference of evaporators according to condenser changes is related to evaporation and is an important factor that has a great influence on the increase of flow rate. Based on this, the flow rate performance prediction according to the change of the $T_{\text{subcooling}}$ of the evaporator was carried out in the modeling. For the reliability of the modeling, the flow rate characteristics were predicted according to the changes of $T_{\text{subcooling}}$ in the fixed FR and the supply heat amount.

In reference to Figure 13 (a), (b), the change in $T_{\text{subcooling}}$ is found through modeling that it is highly related to the flow rate. Both condensers show a tendency to increase the flow rate with the decrease of $T_{\text{subcooling}}$ in the same condition, and when compared with the actual experiment in the same condition, the flow rate of about 1 ~ 2 g/s increased in $T_{\text{subcooling}} = 20^{\circ}\text{C}$. This shows that the factors affecting the flow rate improvement of loop thermosyphon are the supply heat amount, FR, and $T_{\text{subcooling}}$. These three factors can be said to have a great effect on flow characteristics because the higher the supply heat amount, the larger the FR, and the smaller the $T_{\text{subcooling}}$, the higher the amount of evaporation and evaporation frequency.

3. Loop thermosyphon flow instability

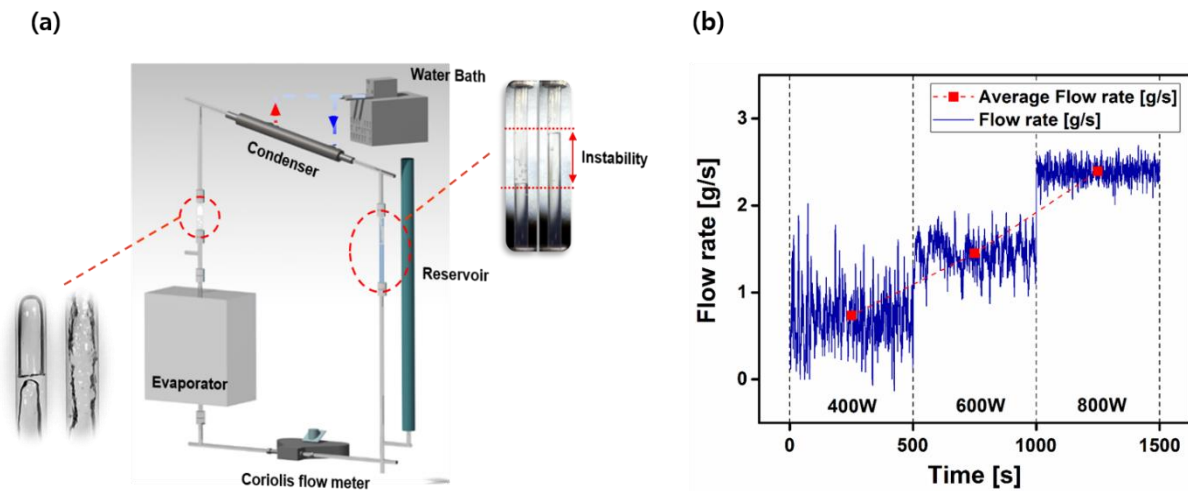


Figure 14. Loop thermosyphon flow instability

As mentioned earlier, the flow instability of loop thermosyphon is associated with evaporation of working fluids and back flow by gravity in evaporators. When the working fluid evaporates in the evaporator, the water column at the condenser outlet is lowered and when the working fluid returns to the evaporator by the gravity and condensation according to the length of pipe, the water column at the condenser outlet increases. This phenomenon occurs repeatedly and can be seen through in Figure 14 (a).

Also, this flow instability is closely related to the heat amount supplied to the loop thermosyphon. Figure 14 (b) shows the flow rate results according to heat amount. As can see in the picture, for low heat amounts, the flow rate represents very large fluctuation, while the fluctuation gradually decreases as the heat amount increases. This is because the working fluid is small of evaporation in low heat amount and most working fluid show backflow but the effect of evaporation as heat amount increases is larger than the backflow of working fluid.

Based on these flow instability of the loop thermosyphon, the concept of electrical energy harvesting of liquid-solid is proposed based on friction energy between the working fluid and the pipe wall when the height of the water column at condenser outlet is changed. For this purpose, the experiment was conducted as follows.

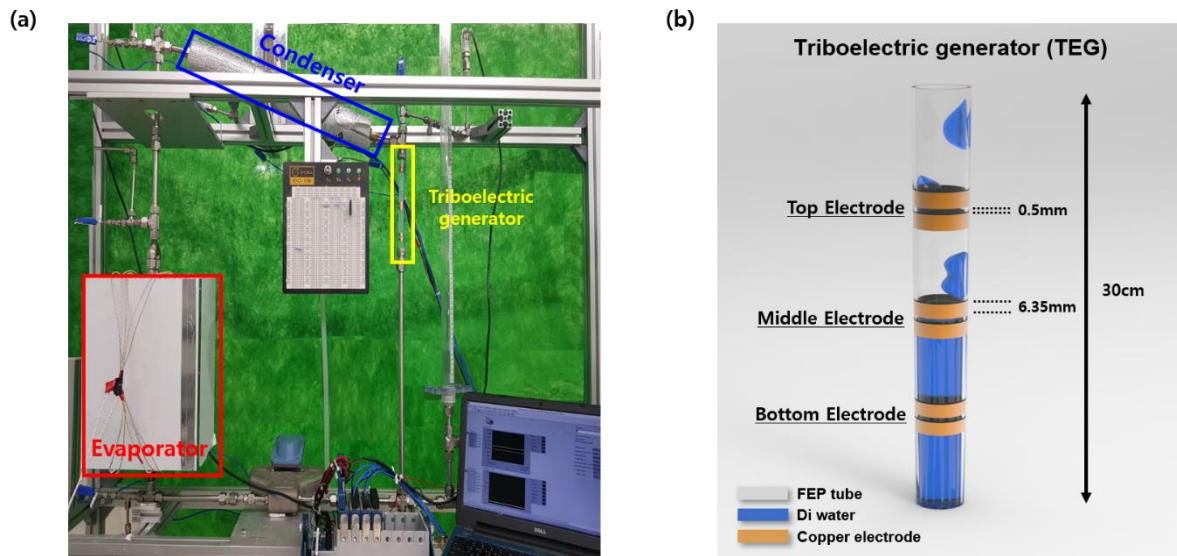


Figure 5. Triboelectric generator applied to the rmosyphon and modeling

An introduction to loop thermosyphon was described in earlier with each component being identical. The shell and tube condenser with high fluctuation of water column was used and Figure15 (a) shows the experiment setup installed the triboelectric generator at condenser outlet. Figure15 (b) shows the 3D modeling of triboelectric generators for the harvest of electrical energy by friction between liquid and solid.

The FEP tube, which has high dielectric constant and hydrophobic characteristics, is a solid insulator and used for electrical energy harvesting, using a condition with an external diameter of 12.7mm and a wall thickness of 1mm. The electrode was attached to the outer wall of the FEP tube with a width of 6.35mm at 0.5mm intervals using a conductive copper tape and three electrodes arrangement were arranged to compare the difference of electrical energy according to the flow pattern of the working fluid.

Except bottom electrode, which is always filled with water, top electrode and middle electrode have two types of friction depending on the flow pattern of the working fluid. In the top electrode, the friction of the droplet shape in which the working fluid directly falls from the condenser outlet and In middle electrode, there are two power generation mechanisms of friction according to change height of water column by flow instability.

3.1. Triboelectric mechanism

There is a description of the electrical energy generation mechanism by two friction that occur between working fluids and triboelectric generator.

Figure 16 shows the electric energy generation mechanism that occurs when a droplet shaped working fluid falling from the condenser outlet is friction with the triboelectric generator. Figure 16 (a) represents an electrical equilibrium state with no effect between working fluid and FEP tube and fluororesin series such as FEP, PVDF and PTFE have a negative pole in the atmosphere because of its high negative polarity. When the surface of FEP tube was partially friction with the droplet, the surface of FEP tube and the droplet formed an interfacial electrical double layer and FEP tube showed negative polarity and relatively Droplet showed positive polarity.

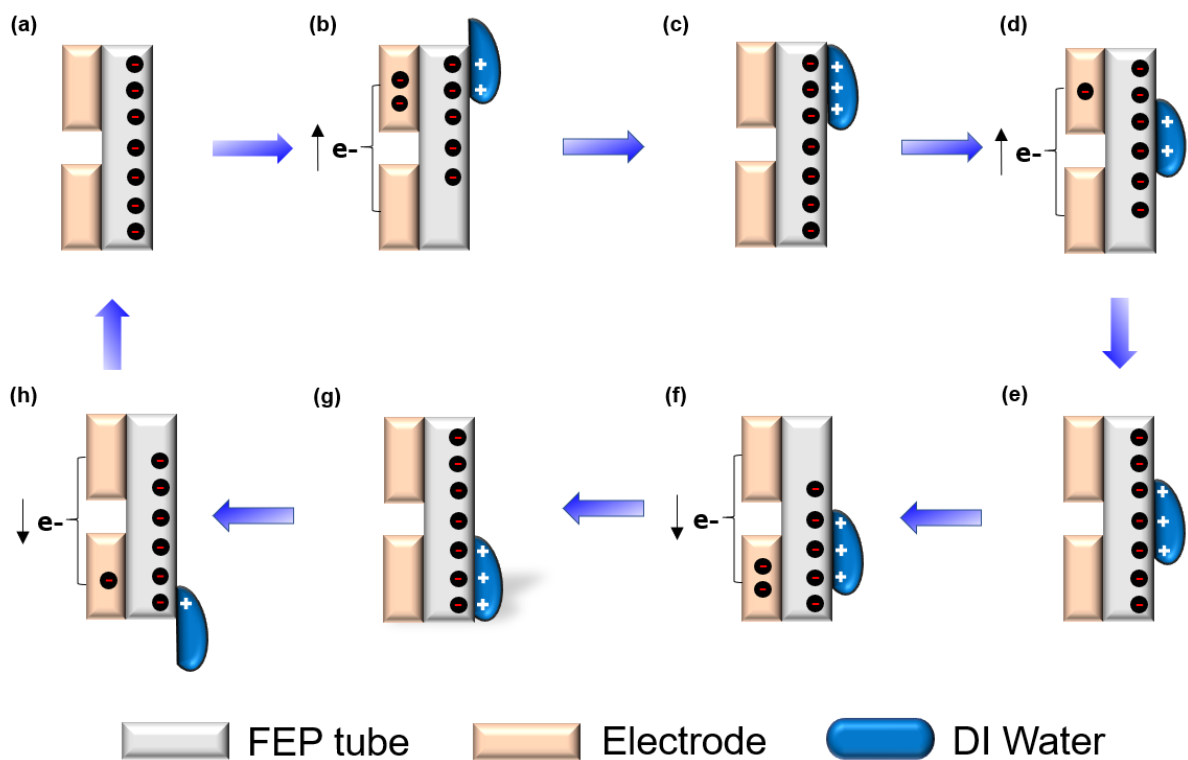


Figure 6 . Voltage generation process of triboelectric generator at top electrode.

As a result, the part partially friction by the electrical double layer becomes an electrical equilibrium that an unbalanced electrical potential difference occurs between the two electrodes and the free electron is moved by the electrostatic induction phenomenon to balance. This movement of free electrons causes electrical energy to occur (Figure 16 b). When an electrical double layer is formed as much as the area of the electrode, it become as electrical equilibrium state as the electrode part, so that not the movement of free electrons and the electrical energy is generated. (Figure 16 c).

Figure 16 (d) generates some unbalanced by potential difference instantaneously as described in Figure 16 (b), and electrical energy is generated by movement of free electrons for electrical equilibrium.

Figure 16 (e) is electrically balanced because the droplet is friction between the two electrodes as same electrical double layer. Therefore, electron movement is not generated and electrical energy is not generated. Figure 16 F ~ h is the same as the mechanism described above and repeats the above process.

In addition to the power generation mechanism by droplets, the electrical generation mechanism of water column by the flow instability of loop thermosyphon is similar to the previously mentioned mechanism.

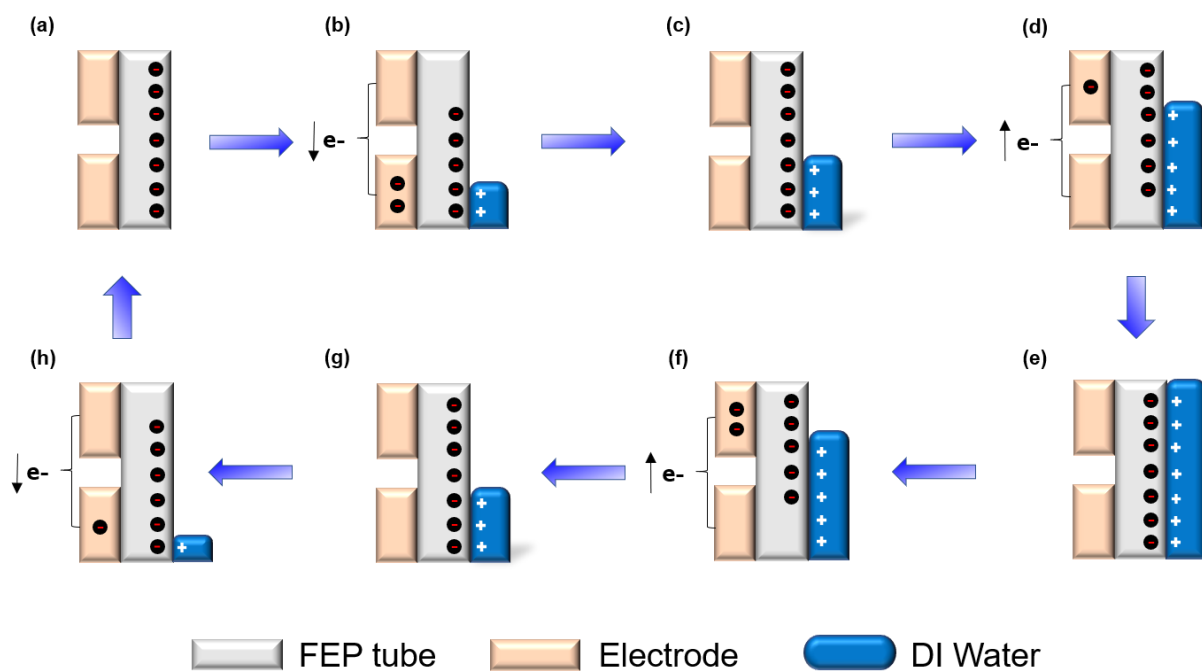


Figure 7. Voltage generation process of triboelectric generator at middle electrode

The electrical generation mechanism by water column occurs that electrons are moved across because water column are raised from the bottom up. Figure 17 (a) is the same as the description of Figure 16 (a) and Figure 17 (b) indicates when friction occurs in part with the water column that comes up along the FEP tube. Electrical double layer is formed as much as the friction area, which becomes electrical equilibrium and causes the free electron to move to the bottom electrode due to unbalanced potential difference. In Figure 17 (c), The working fluid rubs against all electrode areas and is in perfect equilibrium state, so there is no movement of free electrons and no electrical energy. And then when the water column was even higher, the lower electrode is in perfect equilibrium with full contact with water, while the upper electrode is only partially in contact with water and the FEP tube, resulting in an unbalanced potential difference between the electrodes.

Therefore, free electrons are directed upward for electrical equilibrium and electrical energy is generated (Figure 17 d).

In figure 17 (e), the fully risen water column friction against all areas of the two electrodes, resulting in electrical equilibrium and no free electron transfer. The completely filled water column causes friction again as the water column decreases, which causes uneven potential difference of the upper electrode and applies the electrical generation mechanism again (Figure 17 f). Figure 17 (g) and (h) are the same as the mechanism described above and repeats the above process.

These two power generation mechanisms are applied, and in the case of droplets, random electrical energy characteristics are shown due to a large number of droplet but in the case of water columns, electrical energy characteristics with a constant cycle are shown.

3.2. Results and discussions

3.2.1. Comparison of voltage characteristics according to mechanism

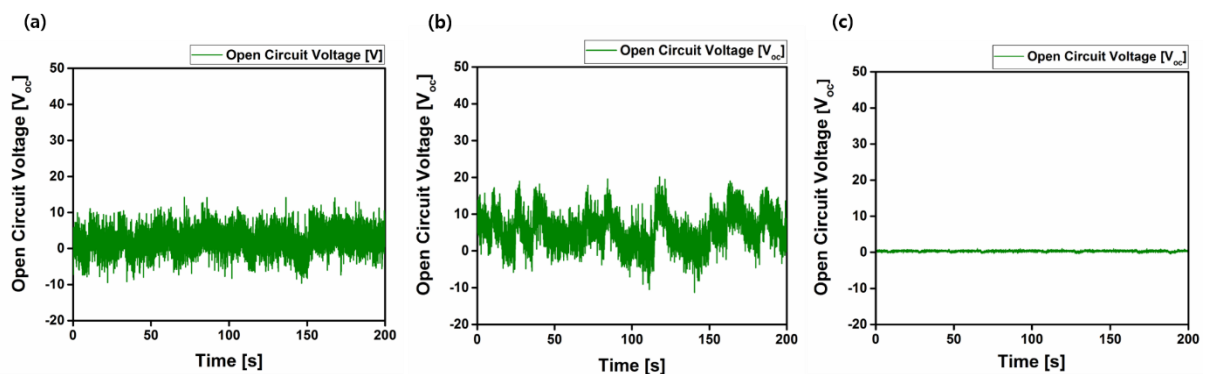


Figure 8. Voltage result according to mechanism

To compare open circuit voltage according electrical generation mechanism above mentioned, the open circuit voltage in each electrode arrangement measured. The open circuit voltage was measured using an electro meter and all experiments were conducted under the same conditions 400W of heat amount and 10 data per second were collected for about 200 seconds in the steady state of loop thermosyphon. Figure 18 (a) represents the open circuit voltage generated in the top electrode, and the voltage result was measured to be constant without change because the condensed working fluid at the condenser outlet randomly drops. On the other hand, Figure 18 (b) shows the open circuit voltage in the middle electrode and unlike Droplet case, it can be seen that the amplitude of the voltage result appears according to the water column change. Figure 18 (c) shows the voltage results at the electrode where water is always filled, and as described above, there is no friction, so there is no electron movement and no voltage generated.

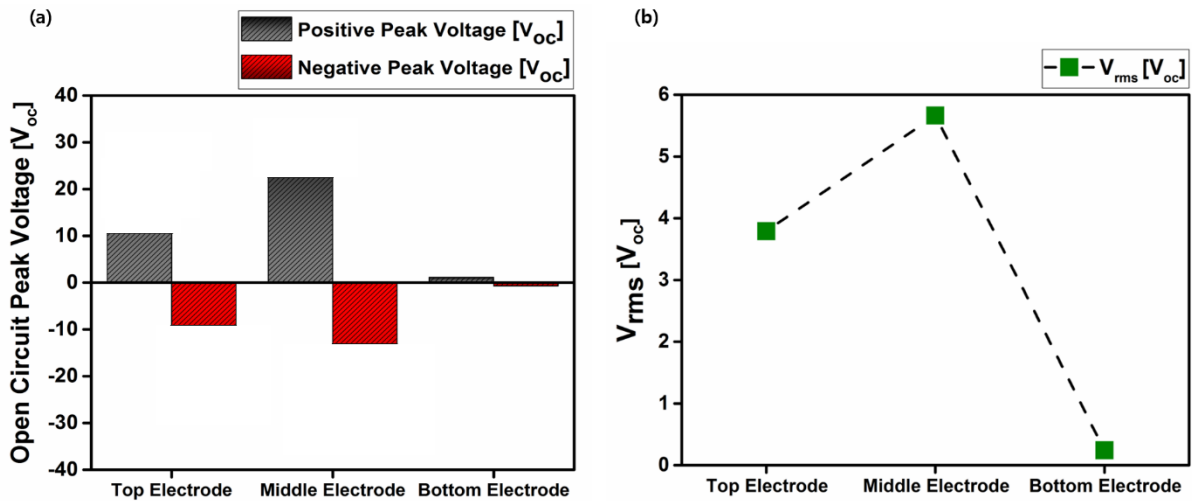


Figure 9. Peak to Peak and V_{rms} result

To investigate the characteristics of the open circuit voltage according to the electrode arrangement in Figure 18, the peak to peak voltage were compared. In Figure 19 (a), when top electrode and middle electrode were compared, the minimum and maximum values of the voltage were higher in the middle electrode. This shows that friction of the working fluid and the FEP tube is more beneficial to the voltage generation when friction occurs in all areas by water column than partially friction by droplet.

Also, the voltage generated by the two mechanisms has the characteristic of the AC voltage. In the case of the AC voltage, since the waveform rate continuously changes, the instantaneous voltage value changes. Figure 19 (b) shows conversion results of DC voltage from AC voltage. It can be seen that higher electric energy is generated in the middle electrode even in DC voltage and matches the AC voltage trend.

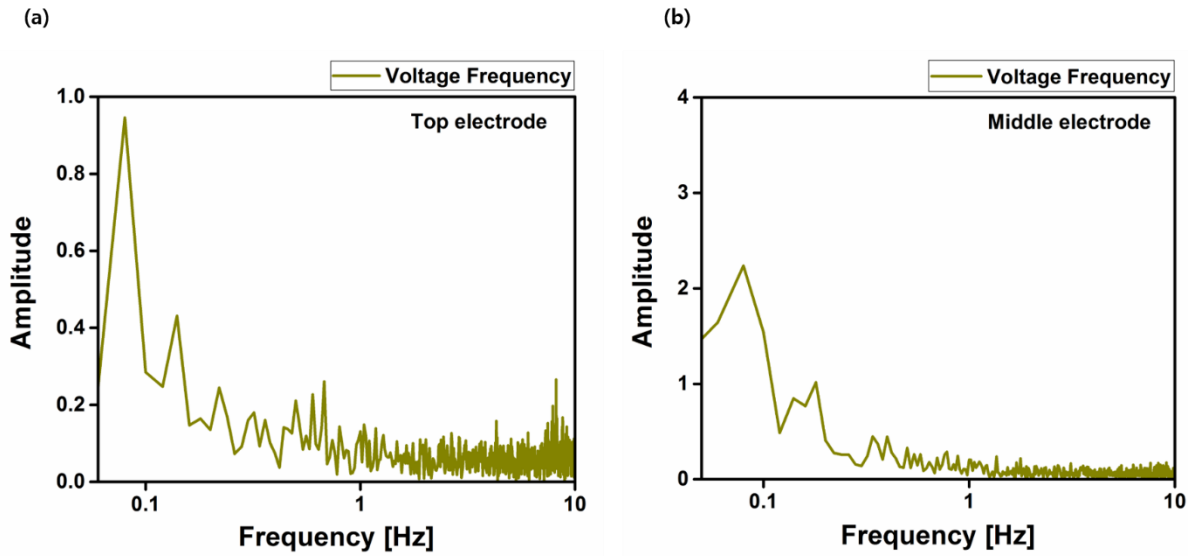


Figure 20. FFT results for voltage generation

However, the peak voltage of the middle electrode showed a low generation frequency in previous results and to confirm this, compared the FFT for each electrode arrangement. The y-axis represents the amplitude according to the magnitude of the voltage result and the x-axis represents the voltage generation frequency.

Figure 20 (a) shows the voltage generation frequency at the top electrode, which shows a low amplitude due to the relatively low voltage, but a constant voltage of about a 0.25 voltage amplitude with 10 Hz is generated. On the other hand, the middle electrode showed a high voltage amplitude but a very low voltage generation frequency.

In the top electrode, a low voltage is generated but the generation frequency is high and the middle electrode generates a high voltage but the generation frequency is low.

3.2.2. Comparison of open circuit voltage with wall thickness

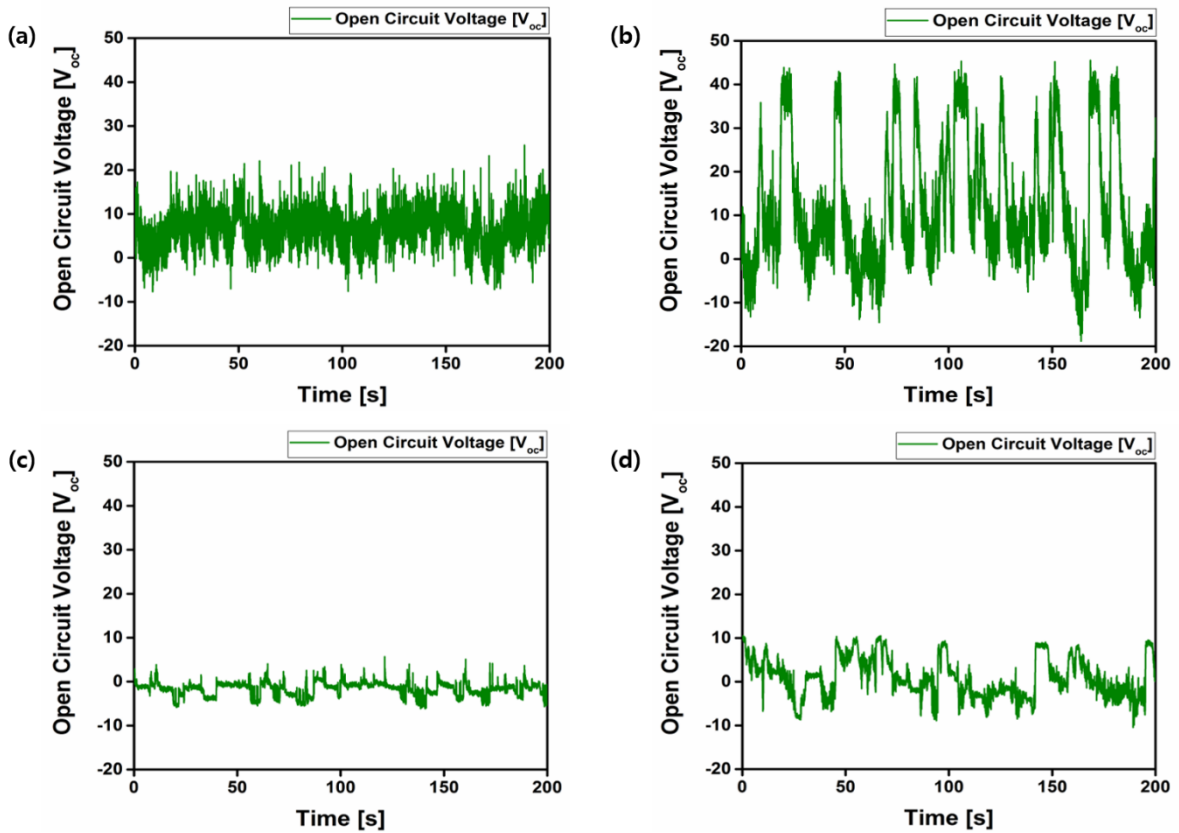


Figure 21. Voltage result according to insulator thickness difference

In order to improve the voltage generated by these two mechanisms, the effect on the voltage result was compared according to the thickness of the insulator.

Figure 21 (a) and (b) show the open circuit voltage results at the top electrode and middle electrode at 0.5 mm FEP tube thickness, and Figures 20 (c) and (d) show the results at 2 mm thickness.

As can be seen from the results, it can be seen that the thinner the thickness of the insulator, the greater the influence on the voltage generation. the difference in the voltage results showed a difference of 15V at the top electrode and 30V at the middle electrode.

This result is due to the fact that the thinner the insulator is the more the negative charge of the FEP tube gets a shorter mutual distance with the positive charge of water. As a result, negative charge and positive charge can cause more surface friction and then More free space of negative charge is generated, so that more free electrons move for electrical equilibrium.

3.2.3. Comparison of open circuit voltage with electrode width

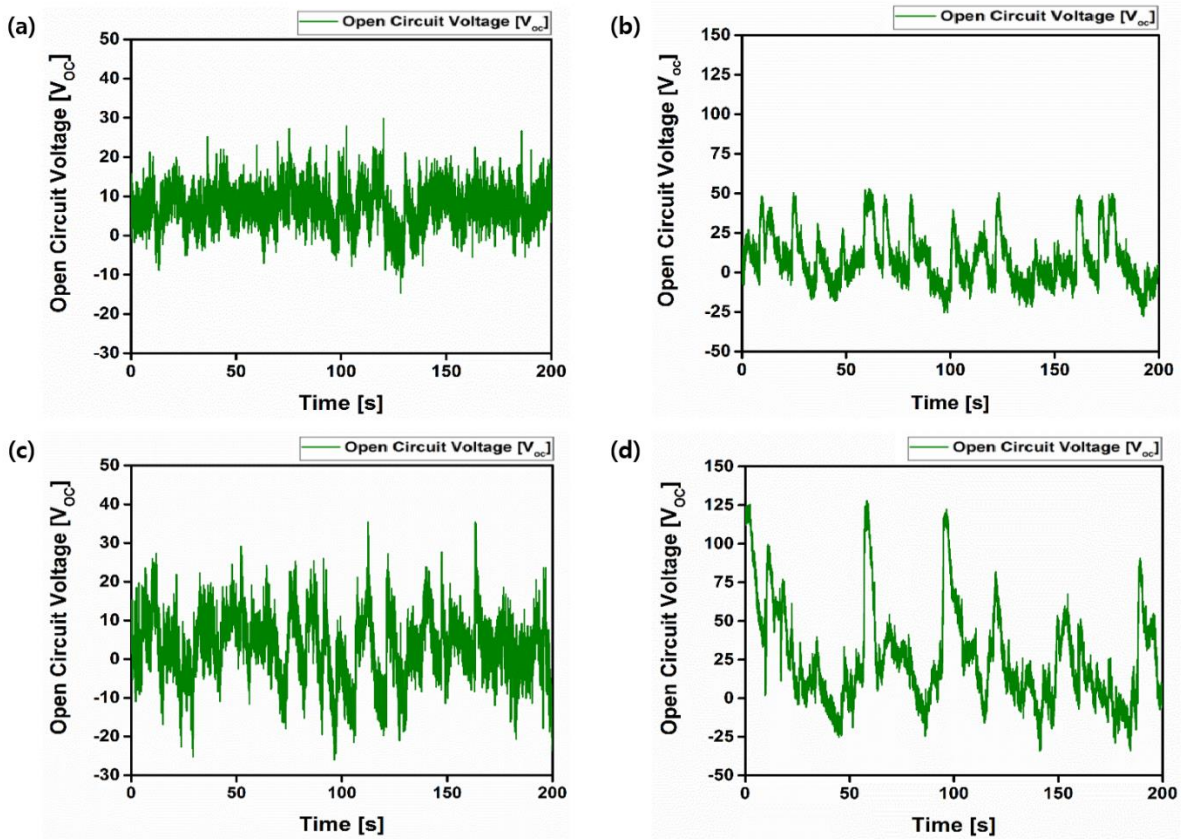


Figure 22. Voltage result according to electrode width

To investigate the effect of electrode width on voltage generation, we compared the results through Figure 21. Figure 22 (a) and (b) show the open circuit voltage results at the top electrode and middle electrode at electrode width 10mm and 0.5 mm FEP tube thickness, and (c) and (d) show the results at electrode width 26mm.

As the electrode width increases, the open circuit voltage increases regardless of the electrode arrangement and the maximum peak voltage reaches 125V at electrode width 26 mm. As the electrode width increases, the space for the free electrons to move can be widened and more can be moved during friction, so that a high voltage result can be obtained.

Therefore, it can be seen that the friction area, the width of the electrode, and the thickness of the insulator are important factors for improving the voltage generation.

3.2.4. Open circuit voltage results of optimized TEG

It can be seen that the thickness of the insulator and the width of the electrode mentioned above are very important factors for the voltage generation. Therefore, based on this, we have fabricated an optimal triboelectric generator that can be applied to loop thermosyphon and conducted experiments.

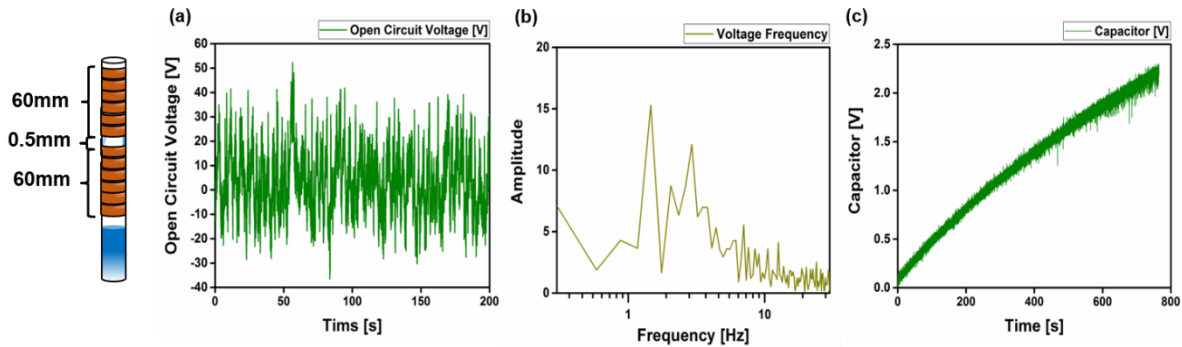


Figure 23. Optimized triboelectric generator characteristics

Figure 23 (a), (b), and (c) show the open circuit voltage, voltage FFT and capacitor charge time for the optimized triboelectric generator. The optimized triboelectric generator was made by 0.5mm of FEP tube wall thickness and 60mm of electrode width in Top Electrode at intervals of 0.5mm and only the droplet generation mechanism is done. voltage generation according to the height change of the water column by flow instability shows a high peak voltage but the voltage generation frequency is very low and the negative voltage and the positive voltage are unbalanced, so the capacitor can not be charged.

Also, voltage generation frequency is decrease than before but this is because the length become longer as the electrode width increases. The highest voltage occurs over a Frequency of more than 1Hz (ie, about -20 or 40V per second), which consumes about 620 seconds to charge a 2V capacitor with 10 μ F.

If many factors that improve the triboelectric energy in addition to factors such as the thickness of the insulator, the electrode width and the friction area are reflect and I think that can harvest higher electrical energy.

3. Conclusion and Future work

Two different types of condensers were applied to the loop thermosyphon to study the behavioral changes of the loop thermosyphon. The changes of operating characteristics were investigated according to the change of FR and the amount of supplied heat amount, and numerical modeling showed that the experimental results and the error probability were less than 5%. Also, suggested the concept of electrical energy production using the friction energy between the working fluid and the FEP tube caused by the flow instability of the thermal system. The mechanism of voltage generation was explained according to the flow characteristics of the working fluid and the characteristics of the finally optimized triboelectric generator were investigated.

The following conclusions are deduced from the present study.

Effect of condenser type change on loop thermosyphon performance.

- In the case of shell and tube condenser, the working fluid evaporated in the evaporator condenses in the condenser and convection heat exchange occurs by the coolant depending on the length. On the other hand, the trapezoid reflux condenser has a coil with a flowing coolant in the center of the condenser and the vapor with low density moves to the space above the condenser, condenses after convection heat exchange and falls downward by gravity. Subsequently, condensed liquid fall by gravity flows along the inclined side. therefore, the condensed liquid will be cooled along its length along the sloped surface, resulting in a temperature difference at the condenser outlet.
- These two condenser differences greatly affect the $T_{\text{subcooling}}$ of evaporator and show a large increase of circulating flowrate in the trapezoid reflux condenser with small $T_{\text{subcooling}}$.
- Numerical modeling of the proposed loop thermosyphon can be used to predict the flow rate and will be able to see the operating characteristics of the loop thermosyphon in various conditions for future testing.

Future work

- Comparison of operating characteristics of loop thermosyphon according to flowrate change of coolant in two condensers.
- Comparison of the operating characteristics of two condensers according to the structure change of loop thermosyphon
- proceeding to the heat amount analysis by considering the coolant flow rate of the condenser in numerical modeling.

Generation of electrical energy by the flow instability of loop thermosyphon.

- Based on the two flow phenomena at the condenser outlet, the results of the open circuit voltage according to the electrode arrangement were measured and characteristics were determined.
- The larger the contact area between the FEP tube and the working fluid, the higher the voltage results and the electrode width and insulate thickness is an important factor in the voltage
- I also confirmed the relevance between flow instability and voltage and presented the possibility of harvesting and charging electric energy by applying optimized triboelectric generator.
- Finally, I extended the applicability and scope of triboelectric generator by applying to system units a range of triboelectric generator that were only being studied on a conventional small scale

Future work

- To increase the friction area between the FEP tube and the working fluid, a method of increasing the surface area of the FEP tube, chemically or physically.
- Since the voltage generation frequency of the triboelectric generator is closely related to the flowrate of the loop thermosyphon, the flowrate increase method through the structural change of the loop thermosyphon and applied to trapezoid reflux condenser.
- Increase voltage method of triboelectric generators using thinner and higher dielectric constant tube increase results.

Reference

- [1] K. Negishi, T. Sawada Heat transfer performance of an inclined two-phase closed thermosyphon *Int. J. Heat Mass Transf.*, 26 (1983), pp. 1207-1213
- [2] A. Faghri, M.M. Chen, M. Morgan Heat transfer characteristics in two-phase closed conventional and concentric annular thermosyphons *Trans. ASME J. Heat Transf.*, 111 (1989), pp. 611-618
- [3] H. Shabgard, B. Xiao, A. Faghri, R. Gupta, W. Weissman Thermal characteristics of a closed thermosyphon under various filling conditions *Int. J. Heat Mass Transf.*, 70 (2014), pp. 91-102
- [4] B. Jiao, L.M. Qiu, X.B. Zhang, Y. Zhang Investigation on the effect of filling ratio on the steady-state heat transfer performance of a vertical two-phase closed thermosyphon *Appl. Therm. Eng.*, 28 (2008), pp. 1417-1426
- [5] H. Imura, K. Sasaguchi, H. Kozai, S. Numata Critical heat flux in a closed two-phase thermosyphon *Int. J. Heat Mass Transf.*, 26 (1983), pp. 1181-1188
- [6] H. Toyoda, T. Nakajima, Y. Kondo, et al. A Design for Loop Thermosyphon Including Effect of Non-condensable Gas *Proceedings of the ASME/JSME 2011 8th Thermal Engineering Joint Conference (March 13–17 2011)*
- [7] R.R. Singh, V. Selladurai, P.K. Ponkarthik, A.B. Solomon Effect of anodization on the heat transfer performance of flat thermosyphon *Exp Therm Fluid Sci*, 68 (2015), pp. 574-581
- [8] V.M. Patel, H.B. Mehta Influence of working fluids on startup mechanism and thermal performance of a closed loop pulsating heat pipe *Appl. Therm. Eng.*, 110 (2017), pp. 1568-1577
- [9] P.R. Pachghare, A.M. Mahalle Effect of pure and binary fluids on closed loop pulsating heat pipe thermal performance *Proc. Eng.*, 51 (2013), pp. 624-629.
- [10] S. Khandekar, Y. Joshi, B. Mehta Thermal performance of closed two-phase thermosyphon using nanofluids *International Journal of Thermal Sciences*, 47 (2008), pp. 659-667
- [11] S.H. Noie, Heat transfer characteristics of a two-phase closed thermosyphon *Appl. Therm. Eng.*, 25 (2005), pp. 495-506
- [12] I. Khazaei, R. Hosseini, S.H. Noie, Experimental investigation of effective parameters and correlation of geyser boiling in a two-phase closed thermosyphon, *Appl. Therm. Eng.*, (2010), pp. 406-412

- [13] R.J. McGlen, R. Jachuck, S. Lin Integrated thermal management techniques for high power electric devices *Appl. Therm. Eng.*, 24 (2004), pp. 1143-1156
- [14] S. Piyush, P. Mike, U. Vivek, et al. Phase change heat transfer device for process heat applications *Nucl. Eng. Des.*, 240 (2010), pp. 2409-2414
- [15] U.C. Kapale, S. Chand Modeling for shell-side pressure drop for liquid flow in shell-and-tube heat exchanger *International Journal of Heat and Mass Transfer*, 49 (2006), pp. 601-610
- [16] Close S. Rozzi, R. Massini, G. Paciello, G. Pagliarini, S. Rainieri, A. Trifiro Heat treatment of fluid foods in a shell and tube heat exchanger: comparison between smooth and helically corrugated wall
- [17] P.G. Vicente, A. García, A. Viedma Mixed convection heat transfer and isothermal pressure drop in corrugated tubes for laminar and transition flow *International Communications in Heat and Mass Transfer*, 31 (2004), pp. 651-662
- [18] Y. Dong, L. Huixiong, C. Tingkuan Pressure drop, heat transfer and performance of single-phase turbulent flow in spirally corrugated tubes *Experimental Thermal and Fluid Science*, 24 (2001), pp. 131-138
- [19] S. Laohalertdecha, S. Wongwiset The effects of corrugation pitch on the condensation heat transfer coefficient and pressure drop of R-134a inside horizontal corrugated tube *International Journal of Heat and Mass Transfer*, 53 (2010), pp. 2924-2931
- [20] J.R. Thome Heat transfer augmentation of shell-and-tube heat exchangers for the chemical processing industry *Journal of Enhanced Heat Transfer*, 4 (2) (1997), pp. 147-161
- [21] R. Hosseini, A. Hosseini-Ghaffar, M. Soltani Experimental determination of shell side heat transfer coefficient and pressure drop for an oil cooler shell-and-tube heat exchanger with three different tube bundles *Applied Thermal Engineering*, 27 (2007), pp. 1001-1008
- [22] W. Roetzel, D. Lee Experimental investigation of leakage in shell-and-tube heat exchangers with segmental baffles *International Journal of Heat and Mass Transfer*, 36 (15) (1993), pp. 3765-3771
- [23] H.D. Li, V. Kottke Effect of the leakage on pressure drop and local heat transfer in shell-and-tube heat exchangers for staggered tube arrangement *International Journal of Heat and Mass Transfer*, 41 (2) (1998), pp. 425-433
- [24] D.A. Reay, P.E. Kew, *Heat pipes (fifth ed.)*, Butterworth-Heinemann, Burlington, USA (2006)
- [25] Zhu, G.; Lin, Z.-H.; Jing, Q. S.; Bai, P.; Pan, C. F.; Yang, Y.; Zhou, Y. S.; Wang, Z. L. Toward

large-scale energy harvesting by a nanoparticle-enhanced triboelectric nanogenerator. *Nano Lett.* 2013, 13, 847–853.

[26] Yang, Y.; Zhu, G.; Zhang, H. L.; Chen, J.; Zhong, X. D.; Lin, Z.-H.; Su, Y. J.; Bai, P.; Wen, X. N.; Wang, Z. L. Triboelectric nanogenerator for harvesting wind energy and as a self-powered wind vector sensor system. *ACS Nano* 2013, 7, 9461–9468.

[27] Wen, X. N.; Yang, W. Q.; Jing, Q. S.; Wang, Z. L. Harvesting broadband kinetic impact energy from mechanical triggering/vibration and water waves. *ACS Nano* 2014, 8, 7405–7412.

[28] Lee, S.; Hong, J. I.; Xu, C.; Lee, M.; Kim, D.; Lin, L.; Hwang, W.; Wang, Z. L. Toward robust nanogenerators using aluminum substrate. *Adv. Mater.* 2012, 24, 4398–4402.

[29] Brown, K. S. Bright future--or brief flare--for renewable energy? *Science* 1999, 285, 678–680.

[30] Dincer, I. Renewable energy and sustainable development: A crucial review. *Renewable Sustainable Energy Rev.* 2000, 4, 157–175.

[31] Lund, H. Renewable energy strategies for sustainable development. *Energy* 2007, 32, 912–919.

[32] Baytekin, H. T.; Patashinski, A. Z.; Branicki, M.; Baytekin, B.; Soh, S.; Grzybowski, B. A. The mosaic of surface charge in contact electrification. *Science* 2011, 333, 308–312.

[33] Baytekin, H. T.; Baytekin, B.; Soh, S.; Grzybowski, B. A. Is water necessary for contact electrification? *Angew. Chem. Int. Ed.* 2011, 50, 6766–6770.

[34] Terris, B. D.; Stern, J. E.; Rugar, D.; Mamin, H. J. Contact electrification using force microscopy. *Phys. Rev. Lett* 1989, 63, 2669.

[35] McCarty, L. S.; Whitesides, G. M. Electrostatic charging due to separation of ions at interfaces: Contact electrification of ionic electrets. *Angew. Chem. Int. Ed.* 2008, 47, 2188–2207

[36] Zhu, G.; Chen, J.; Liu, Y.; Bai, P.; Zhou, Y. S.; Jing, Q. S.; Pan, C. F.; Wang, Z. L. Linear-grating triboelectric generator based on sliding electrification. *Nano Lett.* 2013, 13, 2282–2289.

[37] Lin, Z.-H.; Cheng, G.; Wu, W. Z.; Pradel, K. C.; Wang, Z. L. Dual-mode triboelectric nanogenerator for harvesting water energy and as a self-powered ethanol nanosensor. *ACS Nano* 2014, 8, 6440–6448.

[38] Zhu, G.; Chen, J.; Zhang, T. J.; Jing, Q. S.; Wang, Z. L. Radial-arrayed rotary electrification for high performance triboelectric generator. *Nat. Commun.* 2014, 5, 3426.

- [39] Nguyen, V.; Yang, R. S. Effect of humidity and pressure on the triboelectric nanogenerator. *Nano Energy* 2013, 2, 604–608.
- [40] Bai, P.; Zhu, G.; Liu, Y.; Chen, J.; Jing, Q. S.; Yang, W. Q.; Ma, J. S.; Zhang, G.; Wang, Z. L. Cylindrical rotating triboelectric nanogenerator. *ACS Nano* 2013, 7, 6361–6366.
- [41] Lin, Z. H.; Cheng, G.; Lin, L.; Lee, S.; Wang, Z. L. Water-solid surface contact electrification and its use for harvesting liquidwave energy. *Angew. Chem. Int. Ed.* 2013, 52, 12545–12549.
- [42] Chisholm D (1979) Two-phase flow in bends. *Int. J. Multiphase Flow* 6, 363–367
- [43] Tullis, B. P. and S. C. Robinson.; Quantifying culvert exit loss, *Journal of Irrigation and Drainage Engineering*, 134 (2008)), pp.263-266.
- [44] J. Collier.; *Convective Boiling and Condensation* McGraw Hill Book Company, London, UK (1972)
- [45] W.H. McAdams.; *Heat Transmission* (third ed.), McGraw Hill Book Company, New York (1954)
- [46] S. Zivi.; Estimation of steady-state void fraction by means of the principle of minimum energy production *ASME J. Heat Transf.*, 86 (1964), pp. 247-252
- [47] H. Muller-Steinhagen.; K. Heck A simple friction pressure drop correlation for two-phase flow pipes *Chem. Eng. Process.*, 20 (1986), pp. 297-308

Acknowledgements

I have encountered a lot of difficulties while carrying out my research, but I'm very glad to be able to finish my masters's degree study successfully. In the early days of research, I was worried about how to proceed with the research topic of loop thermosyphon, but interest in the topic grew more and more as ther research was conducted.

First of all, I'm very grateful to my advisor, Professor Jaeson Lee, who has provided me with thorough guidance and generous support for the research to proceed well. Thanks to advisor, I was able to achieve various research results in a short period of time.

I would also like to appreciate Professor Jooha Kim and Gunho Kim for the serious interest and advice on the thesis.

I could complete my study with helps of my laboratory member, so I would like to express my gratitude to them. When I occasionally had obstacles in research, I was able to get good ideas by discussions with the members and get excellent results.

Lastly, I would like to thank my grandmother who watch all these processes from heaven and became a great force when my body and mind were exhausted.

Geunchan Lee